

# A Generalized Theory for Optical Cooling of a Trapped Atom with Spin

Saumitra S. Phatak,<sup>1</sup> Karl N. Blodgett,<sup>2</sup> David Peana,<sup>2</sup> Meng Raymond Chen,<sup>2</sup> and Jonathan D. Hood<sup>3</sup>

<sup>1</sup>*Department of Physics and Astronomy, Purdue University, West Lafayette, Indiana, 47907, USA*

<sup>2</sup>*Department of Chemistry, Purdue University, West Lafayette, Indiana, 47907, USA*

<sup>3</sup>*Department of Physics and Astronomy, Purdue University, West Lafayette, Indiana, 47907, USA,  
Department of Chemistry, Purdue University, West Lafayette, Indiana, 47907, USA\**

(Dated: July 4, 2024)

Cooling atoms to the ground-state of optical tweezers is becoming increasingly important for high-fidelity imaging, cooling, and molecular assembly. While extensive theoretical work has been conducted on cooling in free space, fewer studies have focused on cooling in bound states. In this work, we present a unified formalism for optical cooling mechanisms in neutral atom tweezers, including resolved and unresolved sideband cooling with different trapping potentials, polarization gradient cooling, gray molasses cooling,  $\Lambda$ -enhanced gray molasses cooling, and Raman sideband cooling. We perform simulations and demonstrate good agreement with a simplified spin model. We derive and discuss the fundamental limits of each cooling mechanism and propose new strategies for achieving ground-state cooling in optical tweezers. Our findings provide valuable insights into optimizing cooling schemes for neutral atoms in optical tweezers, paving the way for minimizing thermal decoherence in Rydberg and molecular gates and improving efficiencies of molecular assembly.

## I. INTRODUCTION

Laser cooling of bound neutral atoms has recently gained renewed significance in experiments involving tweezer arrays of atoms and molecules [1]. In systems of Rydberg atoms [2] or molecules [3–5] with dipolar coupling, thermal motion limits the coherence of interactions. Molecular assembly [6, 7] and few-body physics [8, 9] studies require high-fidelity ground-state preparation of multiple atoms.

A wide range of optical cooling techniques have been developed for trapped atoms, illustrated in Fig. 1. Single-photon cooling schemes, such as sideband cooling, have been used for atoms with narrow lines for high-fidelity imaging and ground-state preparation [10–12]. Two-photon schemes, including polarization gradient (PG) [13–16], gray molasses (GM) and  $\Lambda$ -enhanced gray molasses ( $\Lambda$ -GM) [17–21], and Raman-sideband cooling (RSB) [22–26], have been successfully applied for imaging and cooling of atoms without narrow lines. While extensive theoretical work has been developed for sideband cooling [27–29], many of the other cooling schemes for bound atoms are still interpreted through their free-space pictures, for example in Sisyphus cooling where an atom moves through a changing polarization [13]. However, this picture breaks down for a tightly trapped atom in the Lamb-Dicke regime, where the atom wavefunction is smaller than the wavelength.

In this work, we develop a generalized optical cooling model for bound atoms with spin in a single or counter-propagating beam configuration with different polarizations. We validate these models using master equation simulations that include the ground and excited spins

and the harmonic oscillator states. Our analysis reveals a consistent picture across various cooling schemes, shown in Fig. 1. Cooling occurs when  $|n\rangle$  and  $|n-1\rangle$  are Raman coupled for different spin states and brought into resonance using a combination of light shifts (PG, GM,  $\Lambda$ -GM) and two-photon detunings (RSB).

Sideband cooling has been extensively studied in previous works [30, 31], but cooling of a bound atom with spin has been much more limited. Previous work on cooling bound atoms with spin has primarily focused on specific cases, such as  $J=1/2$  to  $J'=3/2$  transitions in counter-propagating orthogonal linear light [32] or linear light with standing waves [33]. We develop a new formalism for arbitrary spin and polarization, with a particular emphasis on the experimentally relevant  $\sigma_+ - \sigma_-$  configuration. Notably, while these previous theoretical studies found a fundamental limit of  $\langle n \rangle \approx 1$ , we demonstrate that schemes like GM and  $\Lambda$ -GM can be used for high ground-state preparation when considering different polarization and spin configurations.

A recent experimental result achieved a record-high imaging fidelity of 99.96% for lithium using  $\Lambda$ -enhanced GM cooling with significant ground-state preparation, despite lithium having the largest recoil heating [21]. This raises the question of whether spin cooling techniques can be further optimized for ground-state preparation. The unified model also allows us to explore novel cooling schemes that transcend the conventions of any single conventional cooling technique.

The paper is structured as follows. Section II develops the general master equation for spin cooling and derive effective ground-state spin operators by adiabatically eliminating the excited state. Section III applies this formalism to sideband cooling, including cases with different excited state trapping frequencies. Section IV develops a formalism for spin cooling and applies it to PG, GM,  $\Lambda$ -GM, and RSB cooling. Each section compares exact

\* hoodjd@purdue.edu

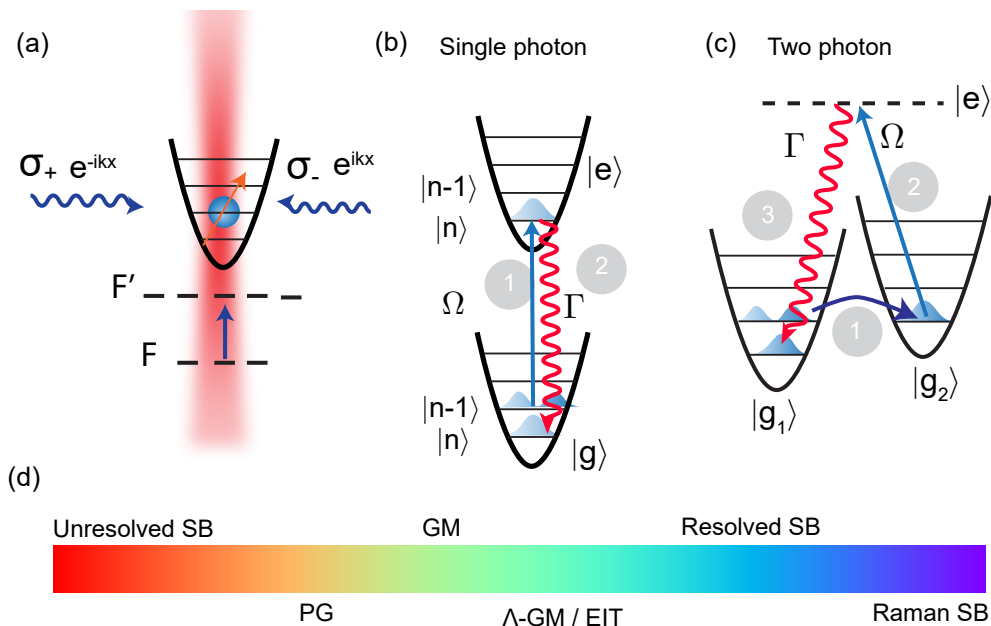


FIG. 1. (a) Laser cooling of a trapped atom with ground and excited state spin  $F$  and  $F'$  in a changing polarization from counter-propagating beams. (b) Single photon cooling schemes such as resolved and unresolved sideband cooling drive population from the ground-state to the excited state with one reduced motional quanta  $n - 1$ . In the Lamb-Dicke regime, the recoil heating is smaller than the trapping frequency and the population mostly returns to  $n - 1$ , resulting in net cooling. (c) Two-photon cooling schemes like polarization gradient (PG), gray molasses (GM), and  $\Lambda$ -enhanced gray molasses ( $\Lambda$ -GM) drive  $n \rightarrow n - 1$  between two ground-state spins with a two-photon Raman transition. (d) Temperature scale for cooling schemes. A wide variety of cooling schemes have been used to trap, cool, and image tightly trapped atoms.

simulations to simplified models and contrasts various cooling techniques, with the goal of creating a unified picture that will lead to more coherent interactions and higher fidelity ground-state preparation.

## II. THEORY: LASER COOLING IN A HARMONIC POTENTIAL

### A. Master equation for laser cooling

In this section, we develop a master equation for an atom confined in a tight harmonic trap and interacting with a semi-classical electric field. In a semi-classical approximation, we take the expectation of the electric field but keep the atom position  $\hat{x}$  as a quantum operator [34, 35]. The electric field for a single laser frequency  $\omega_L$  is

$$\mathbf{E}(\hat{x}, t) = E_0 \boldsymbol{\epsilon}(\hat{x}) e^{-i\omega_L t} + h.c.. \quad (1)$$

$E_0$  is a real field amplitude and the last term is the hermitian conjugate. The complex polarization and phase are contained within  $\boldsymbol{\epsilon}(\hat{x})$  and can describe a traveling wave or a standing wave with various polarization configurations.

The atom has ground hyperfine spin states denoted as  $|F_g m_g\rangle$  and excited hyperfine spin states denoted as

$|F_e m_e\rangle$ . The ground and excited state projection operators  $P_e$  are

$$P_e = \sum_{m_e} |F_e m_e\rangle \langle F_e m_e|$$

$$P_g = \sum_{m_g} |F_g m_g\rangle \langle F_g m_g|. \quad (2)$$

For an optically trapped atom, the ground and excited states can generally experience different potentials due to their differing polarizabilities. This difference will be addressed later, but for now, we will assume that the ground and excited states share the same harmonic trapping frequency  $\nu$ . The total Hamiltonian for the bound atom interacting with the electric field in the rotating frame of the laser is [34, 35]

$$\hat{H} = \nu \hat{a}^\dagger \hat{a} + \left( \Delta - i \frac{\Gamma}{2} \right) P_e - \frac{\Omega}{2} \left( \boldsymbol{\epsilon}(\hat{x}) \cdot \hat{\mathbf{D}}^\dagger + h.c. \right). \quad (3)$$

$\Delta = \omega_A - \omega_L$  is the detuning of the atom from the laser. The Rabi frequency  $\Omega$  is defined in terms of the reduced matrix element times the electric field amplitude

$$\Omega = \langle J_e || d || J_g \rangle E_0 / \hbar. \quad (4)$$

The atomic operator  $\hat{\mathbf{D}}^\dagger$  is a raising operator for all the hyperfine levels in the ground-state, and  $\hat{\mathbf{D}}$  is the corresponding lowering operator. They are defined in terms of

the dipole operator  $\hat{\mathbf{d}}$  normalized by the reduced matrix element,

$$\hat{\mathbf{D}} = \frac{P_g \hat{\mathbf{d}} P_e}{\langle J_e || \hat{\mathbf{d}} || J_g \rangle}, \quad \hat{\mathbf{D}}^\dagger = \frac{P_e \hat{\mathbf{d}} P_g}{\langle J_e || \hat{\mathbf{d}} || J_g \rangle}. \quad (5)$$

The Hamiltonian in Eq. 3 also contains a non-Hermitian imaginary decay rate  $\Gamma$  of the excited state due to spontaneous emission. In the Wigner-Weisskopf model, the excited state decays due to spontaneous emission without repopulating the ground-state. This leads to a reduction in the wavefunction normalization. The master equation for the density matrix contains refeeding terms with collapse operators  $L_i$  that repopulate the ground-state and preserve the density matrix normalization:

$$\frac{d\hat{\rho}}{dt} = -i(\hat{H}\hat{\rho} - \hat{\rho}\hat{H}^\dagger) + \sum_i \hat{L}_i \hat{\rho} \hat{L}_i^\dagger. \quad (6)$$

The collapse operators contain both the lowering of the excited state as well as the momentum recoil for emitting a photon:

$$\hat{L}_{\hat{\mathbf{n}},q} = \sqrt{\Gamma} \hat{R}_{\mathbf{n},q} \hat{D}_q. \quad (7)$$

The collapse operators have two effects when operating on the density matrix. First, they lower the atom back to the ground-state.  $\hat{D}_q$  is the lowering operator in the spherical vector basis  $\hat{D}_q = \hat{\mathbf{e}}_q^* \cdot \hat{\mathbf{D}}$ , where  $\hat{\mathbf{e}}_q$  is a spherical basis vector. Second, the recoil operator  $\hat{R}_{\mathbf{n},q}$  imparts a momentum kick due to the photon recoil after the emission of a photon with polarization  $q$  in  $\mathbf{n}$  directions. In general, the recoil operator is averaged over the angular emission profile for each polarization. If we assume that the photon is emitted along either direction of the  $x$ -axis, then the recoil operators are  $R_{\pm,q} = e^{\pm ikx}$ , and we have a total of six collapse operators for the two emissions directions and three polarizations

$$\hat{L}_{\pm,q} = \sqrt{\Gamma} e^{\pm ik\hat{x}} \hat{D}_q. \quad (8)$$

In 1D, the photon recoil operator  $R_{\pm} = e^{\pm ik\hat{x}}$  can be understood as a momentum translation operator that induces a momentum kick due to the recoil from an emitted photon, with  $e^{\pm ik\hat{x}} |\psi(p)\rangle = |\psi(p \pm \hbar k)\rangle$ .

We can express the position operator in terms of the harmonic oscillator creation and annihilation operators  $\hat{x} = x_0(\hat{a} + \hat{a}^\dagger)$ , where  $x_0 = \sqrt{\hbar/2m\nu}$  is the width of the ground-state wavefunction. The recoil operator becomes  $e^{ik\hat{x}} = e^{i\eta(\hat{a} + \hat{a}^\dagger)}$ , where the Lamb-Dicke (LD) parameter  $\eta = kx_0$  is the ratio of the ground-state wavefunction width to the wavelength.

The square of the LD parameter also happens to be equal to the ratio of the photon recoil energy  $E_{\text{recoil}} = \hbar^2 k^2 / (2m)$  to the harmonic energy  $\hbar\nu$ , or  $\eta^2 = E_{\text{recoil}} / (\hbar\nu)$ . When  $\eta \ll 1$ , then the recoil from photon emission or absorption is unlikely to change  $n$ , and the ground-state wavefunction is smaller than the

cooling laser's wavelength. In this regime, we can also approximate the recoil operator as

$$e^{ik\hat{x}} \approx 1 + i\eta(\hat{a} + \hat{a}^\dagger). \quad (9)$$

The result of a recoil is then  $e^{ik\hat{x}} |n\rangle \approx |n\rangle + \eta\sqrt{n}|n-1\rangle + \eta\sqrt{n+1}|n+1\rangle$ . The zeroth order term is from  $n \rightarrow n$ , and the first order LD term is from  $n \rightarrow n \pm 1$ . The LD regime is defined as when  $\eta^2(2n+1) \ll 1$ . One common misconception is that in the LD regime, heating is suppressed. Although the probability of  $n$  changing decreases, the overall heating rate is still given by the scattering rate times the recoil energy.

More generally, the matrix element can be expressed in terms of the generalized Laguerre polynomial as [36]

$$\langle n' | e^{ik\hat{x}} | n \rangle = e^{-\eta^2/2} \left( \frac{n_{<}!}{(n_{<} + \Delta n)!} \right)^{1/2} (i\eta)^{\Delta n} L_{n_{<}}^{\Delta n}(\eta^2). \quad (10)$$

Here,  $n_{<}$  is the least of  $n$  and  $n'$ , and  $\Delta n = |n' - n|$ . This functional form becomes important when cooling outside the LD regime. The  $n \rightarrow n-1$  transition goes to zero for higher  $n$ , creating dark motional states where the population gets stuck. Cooling can still occur by addressing higher order sidebands, as shown experimentally in Ref. [26].

The master equation here is simulated throughout this paper for different cooling schemes using the steady-state solver in QuTip [37]. We include up to 15 harmonic states, which for the larger spin systems in this paper like  $F=1$  to  $F=2$  takes approximately one minute per simulation.

## B. Effective master equation within ground-state subspace

Most optical cooling processes take place when there is low saturation, meaning that only a small amount of the steady-state population is in the excited state. The excited state can then be reasonably approximated from the ground state, and can be adiabatically eliminated. In this section, we will derive the effective ground-state master equation.

In situations where the excited state quickly reaches an equilibrium, the excited state can be solved in terms of the ground-states and then eliminated from the time evolution equations. The elimination results in an effective Hamiltonian and collapse operator that gives the dynamics within the ground-state. These effective operators can be derived by performing these operations for a given Hamiltonian [38], but Ref. [39] provides a compact general formalism that we use here.

This first form is valid even when the cooling light is close to resonance such as in sideband cooling. The Hamiltonian and collapse operators within the ground-

state subspace are

$$H_{\text{eff}} = \nu a^\dagger a - \frac{1}{2} \left[ \sum_{m_g, m_e} \frac{P_g H |m_e\rangle \langle m_e| H |m_g\rangle \langle m_g|}{(\Delta_{m_e, m_g} - i\Gamma/2)} + h.c. \right] \quad (11)$$

$$L_{\text{eff}}^i = L_i \sum_{m_g, m_e} \frac{|m_e\rangle \langle m_e| H |m_g\rangle \langle m_g|}{\Delta_{m_e, m_g} - i\Gamma/2}. \quad (12)$$

Here the laser detuning is  $\Delta_{m_g, m_e} = \omega_L - (E_{m_e} - E_{m_g})$  appears in the denominator. For the case of an atom with spin interacting with a single frequency laser field, as in the Hamiltonian in Eq. 3, the effective ground-state Hamiltonian is

$$H_{\text{eff}} = \nu \hat{a}^\dagger \hat{a} - \frac{\Omega^2}{8} \left[ \sum_{m_g, m_e} \frac{(\boldsymbol{\epsilon}(\hat{x}) \cdot \mathbf{D}) |m_e\rangle \langle m_e| (\boldsymbol{\epsilon}^*(\hat{x}) \cdot \mathbf{D}^\dagger) |m_g\rangle \langle m_g|}{\Delta_{m_g, m_e} - i\Gamma/2} + h.c. \right] \quad (13)$$

and the collapse operator for the emission of a photon with polarization  $q$  is:

$$L_{\text{eff}}^{q, n} = -\sqrt{\Gamma} \frac{\Omega}{2} \sum_{m_g, m_e} \frac{(\mathcal{R}_n \mathbf{e}_q^* \cdot \mathbf{D}) |m_e\rangle \langle m_e| (\boldsymbol{\epsilon}(\hat{x}) \cdot \mathbf{D}^\dagger) |m_g\rangle \langle m_g|}{\Delta_{m_g, m_e} - i\Gamma/2}. \quad (14)$$

The effective Hamiltonian includes light shifts, two-photon Raman coupling, and decay due to spontaneous emission. The collapse operators repopulate the ground-state.

Two photon cooling schemes operate in the large detuning limit. In the large detuning limit, the state dependence in the denominator detuning vanishes  $\Delta_{m_g, m_e} \approx \Delta$ . The sum over the excited states in the numerator becomes the identity. The effective ground-state operators simplify to:

$$H_{\text{eff}} = \nu a^\dagger a - \frac{1}{2\Delta} (P_g H P_e H P_g) \quad (15)$$

$$L_{\text{eff}}^q = L_q \frac{P_e H P_g}{\Delta - i\Gamma/2}. \quad (16)$$

For the single frequency Hamiltonian in Eq. 3, it becomes

$$H_{\text{eff}} = \nu \hat{a}^\dagger \hat{a} - \frac{\Omega^2}{4\Delta} [(\boldsymbol{\epsilon}^*(\hat{x}) \cdot \mathbf{D})(\boldsymbol{\epsilon}(\hat{x}) \cdot \mathbf{D}^\dagger)] \quad (17)$$

and the ground-state collapse operator in the large detuning limit is

$$L_{\text{eff}}^{q, n} = -\sqrt{\Gamma} \frac{\Omega}{2} \left[ \frac{(\mathcal{R}_n \hat{\mathbf{e}}_q^* \cdot \mathbf{D})(\boldsymbol{\epsilon}(\hat{x}) \cdot \mathbf{D}^\dagger)}{\Delta - i\Gamma/2} \right]. \quad (18)$$

The interaction part of the ground-state Hamiltonian describes two-photon processes such as light shifts and Raman transitions. The right term in the numerator

$\boldsymbol{\epsilon}(\hat{x}) \cdot \hat{\mathbf{D}}^\dagger$  excites the atom due to absorption of a photon from the cooling light. The left term  $\boldsymbol{\epsilon}^*(\hat{x}) \cdot \hat{\mathbf{D}}$  returns the atom to the ground-state with the emission of a photon into the cooling light.

The ground-state collapse operator describes the redistribution of population within the ground-state due to spontaneous emission. It has a similar form compared to interaction Hamiltonian. The right term  $\boldsymbol{\epsilon}(\hat{x}) \cdot \hat{\mathbf{D}}^\dagger$  excites the atom due to the absorption of a photon from the cooling light. The left term  $\mathcal{R}_n \mathbf{e}_q^* \cdot \hat{\mathbf{D}}$  returns the atom to the ground-state by emitting a photon into free-space and gives the atom a momentum kick through the recoil operator  $\mathcal{R}_n$ . This momentum kick is the key difference between the two operators.

After adiabatic elimination, the form of both the effective Hamiltonian and collapse operators are in terms of the scalar products of the dipole operators and field polarization,

$$H \propto (\mathbf{A}^* \cdot \hat{\mathbf{D}})(\hat{\mathbf{D}}^\dagger \cdot \mathbf{B}) = (\mathbf{A}^* \otimes \mathbf{B}) \cdot (\hat{\mathbf{D}} \otimes \hat{\mathbf{D}}^\dagger). \quad (19)$$

These operators act within the ground-state spin manifold just like the hyperfine spin operators  $\hat{F}_i, F_\pm$ . If you observe, the right hand side is actually a scalar product of two rank 2 matrices. Using the Wigner-Eckart theorem and properties of spherical vectors, we can express these in terms of spin operators. The spin Hamiltonian is [38]

$$H_{\text{eff}} = \nu \hat{a}^\dagger \hat{a} - \frac{\Omega^2}{4\Delta} \left[ C^{(0)} |\boldsymbol{\epsilon}(\hat{x})|^2 + C^{(1)} i(\boldsymbol{\epsilon}^*(\hat{x}) \times \boldsymbol{\epsilon}(\hat{x})) + C^{(2)} \left( ((\boldsymbol{\epsilon}^*(\hat{x}) \cdot \hat{\mathbf{F}})(\boldsymbol{\epsilon}(\hat{x}) \cdot \hat{\mathbf{F}}) + c.c.)/2 - \frac{1}{3} \hat{\mathbf{F}}^2 |\boldsymbol{\epsilon}(\hat{x})|^2 \right) \right] \quad (20)$$

and the collapse operators which give the redistribution of population in the ground-state due to spontaneous emission are

$$L_{\text{eff}} = -\sqrt{\Gamma} \frac{\Omega}{2\Delta} \left[ C^{(0)} (\mathcal{R}_n \hat{\mathbf{e}}_q^*) \cdot \boldsymbol{\epsilon}(\hat{x}) + C^{(1)} i((\mathcal{R}_n \hat{\mathbf{e}}_q^*) \times \boldsymbol{\epsilon}(\hat{x})) + \frac{C^{(2)}}{2} \left[ ((\mathcal{R}_n \hat{\mathbf{e}}_q^* \cdot \hat{\mathbf{F}})(\boldsymbol{\epsilon}(\hat{x}) \cdot \hat{\mathbf{F}}) + c.c.) - \frac{1}{3} \hat{\mathbf{F}}^2 |(\mathcal{R}_n \hat{\mathbf{e}}_q^*) \cdot \boldsymbol{\epsilon}(\hat{x})| \right] \right]. \quad (21)$$

The effective spin operators are valid for any ground and excited spin states. The excited state only affects the  $C^{(i)}$  coefficients.

The ground-state collapse operators in Eqs. 18 (far detuned limit) and 14 (near-resonant limit) describe the redistribution of the population within the ground-state. With the effective ground-state Hamiltonian, a master equation incorporating these operators describes the ground-state dynamics. The Hamiltonian accounts for energy shifts and coherent transfer between states, while

the collapse operators account for incoherent redistribution due to spontaneous emission.

Next, we will derive an approximate population rate equation by working in the basis where  $H_{\text{eff}}$  is diagonal. We define an interaction picture by applying a unitary transformation  $\tilde{A} = UAU^\dagger$  with  $U = e^{-iH_{\text{eff}}t}$ . In the interaction picture, the time evolution of the Hamiltonian is included within the density matrix and operators  $U\rho U^\dagger$  with unitary  $U = e^{-iHt}$ . In the interaction picture, the master equation is:

$$\dot{\tilde{\rho}} = \sum_q \left[ \tilde{L}_{\text{eff},q} \tilde{\rho} \tilde{L}_{\text{eff},q}^\dagger - \frac{1}{2} \{ \tilde{L}_{\text{eff},q}^\dagger \tilde{L}_{\text{eff},q}, \tilde{\rho} \} \right]. \quad (22)$$

Finally, we derive rate equations for the populations by multiplying by  $\langle n |$  on the left and  $|n\rangle$  on the right and defining the populations  $P(n) = \tilde{\rho}_{nn} = \rho_{nn}$ . The resulting equation contains coherence terms  $\langle n | \rho | m \rangle$  between ground-states. If we work in the basis where the ground-state Hamiltonian is diagonal, these coherences are less important and can often be ignored. By setting all these coherences to zero, we obtain a population rate equation:

$$\frac{dP(n)}{dt} = -P(n) \sum_m \gamma_{n \rightarrow m} + \sum_m \gamma_{m \rightarrow n} P(m), \quad (23)$$

where the transfer rate between ground-states  $n$  and  $m$  is:

$$\gamma_{n \rightarrow m} = \sum_q |\langle m | L_{\text{eff},q} | n \rangle|^2. \quad (24)$$

Note that in this last equation,  $L_{\text{eff}}$  can be taken out of the interaction picture because as long as  $n$  and  $m$  are eigenstates of  $H_{\text{eff}}$ , the time-dependence cancels upon taking the magnitude. However, it is important to remember that the eigenstates must be those of  $H_{\text{eff}}$ . The steady-state conditions can then be found by solving the matrix equation for  $\frac{dP(n)}{dt} = 0$ . In this paper, we derive analytic solutions for different cooling schemes by picking an appropriate basis where the coherences between eigenstates are least important and solving this rate equation.

To compare different cooling schemes we need to set some parameter as a metric. The energy or temperature of a single atom confined in a 1D harmonic potential is given by  $E = \hbar\nu(\langle n \rangle + 1/2)$ , where  $\nu$  is the trapping frequency, and  $\langle n \rangle$  is the average motional quantum number. However, it is important to note that the energy of a single atom in an optical tweezer can be manipulated by adiabatically varying the optical trap power [14], where both the trapping frequency and the energy scale with the square root of the optical trap power. As a result, the motional quantum number,  $\langle n \rangle$ , becomes a more relevant quantity to consider, as it remains conserved during adiabatic changes in the trap depth. Therefore, we choose to use  $\langle n \rangle$  as the cooling metric for comparing all the techniques in the following discussions.

### III. SIDEBAND COOLING

For an atom confined in a harmonic trap within the Lamb-Dicke (LD) regime, Doppler cooling operates differently than in free space, as illustrated in Fig. 2(a). In this scenario, the cooling laser drives transitions from the motional state  $n$  to  $n-1$ , while spontaneous emission predominantly returns the atom to the  $n-1$  state. This process leads to net cooling because, in the LD regime, the recoil energy from photon emission is smaller than the energy spacing between trap levels ( $\hbar\nu$ ). Doppler cooling of trapped atoms can be classified into two regimes based on the relationship between the trapping frequency  $\nu$  and the atomic transition linewidth  $\Gamma$ :

- Resolved sideband cooling: when  $\nu > \Gamma$
- Unresolved sideband cooling: when  $\nu < \Gamma$

These regimes exhibit distinct cooling dynamics and efficiencies, which we will explore in subsequent sections. Sideband cooling was extensively studied theoretically in the 1980's by Refs. [30, 31, 36, 40]. It has been demonstrated experimentally in ions [29], neutral atoms [41, 42], and nanomechanical oscillators [28]. Here we present these results in our formalism. We then look at the case of different trapping frequencies and derive an analytic expression for the steady-state temperature.

Doppler cooling for a bound atom in the LD regime only requires a single traveling wave  $\epsilon(\hat{x}) = e^{-ik\hat{x}}$ . For a two-level system, the dipole operators are  $\hat{D} = \hat{\sigma} = |g\rangle\langle e|$ . The Hamiltonian is

$$H = \nu\hat{a}^\dagger\hat{a} + \Delta|e\rangle\langle e| - \frac{\Omega}{2} \left( e^{-ik\hat{x}}\hat{D}^\dagger + h.c. \right), \quad (25)$$

and the collapse operators for emission into the positive and negative  $x$ -direction is

$$L_\pm = \sqrt{\Gamma} e^{\pm ikx} \hat{D}. \quad (26)$$

The resonant and spontaneous emission processes are shown in Fig. 2(b). To estimate the final population distribution, we can use the effective ground-state collapse operator in Eq. 14 and the population transfer rates from Eq. 24. From these equations, the transfer rate between ground-states  $n_1$  and  $n_2$  in the ground-state through the excited harmonic states  $n_e$  is

$$\gamma_{n_1 \rightarrow n_2} = \Gamma \Omega^2 \sum_{\pm} \left| \sum_{n_e} \frac{\langle n_2 | e^{\pm ik\hat{x}} | n_e \rangle \langle n_e | e^{ik\hat{x}} | n_1 \rangle}{\Delta + \nu(n_1 - n_e) - i\Gamma/2} \right|^2. \quad (27)$$

The sum inside the magnitude is over the excited state  $n_e$  and pathways through each excited motional state can interfere. The sum on the outside is over the emission direction. Emission into each direction results in a different phase, and the average over all directions averages out the coherences between the different pathways. As a result,

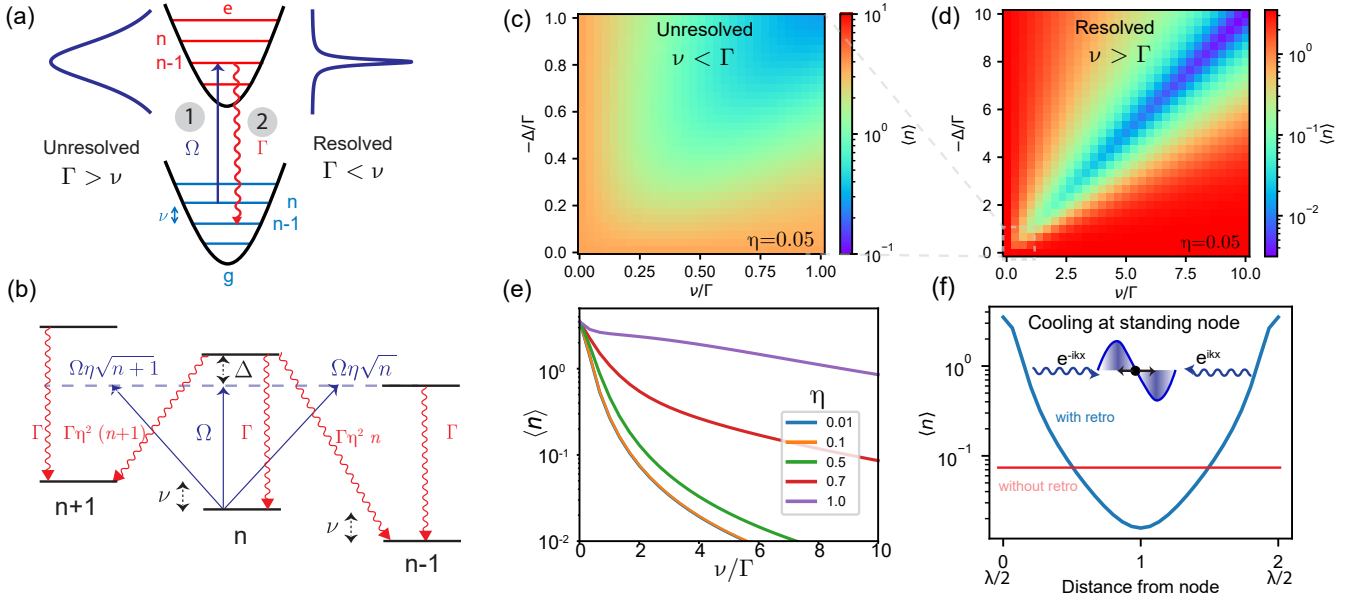


FIG. 2. (a) Resolved ( $\Gamma < \nu$ ) and unresolved ( $\Gamma > \nu$ ) sideband cooling in the Lamb-Dicke regime. (b) The cooling laser drives the three blue transitions. Spontaneous emission (red) most likely does not change  $n$  in the LD regime. (c-d) Simulation of  $\langle n \rangle$  in the unresolved and resolved regime for  $\eta = 0.05$ . (e) The population versus trapping frequency. (f) Cooling in a standing wave can lower the energy by positioning the atom at the node, thereby decreasing scattering.

we can take the sum over the excited states outside of the sum and omit the average over directions,

$$\gamma_{n_1 \rightarrow n_2} = \Gamma \Omega^2 \sum_{n_e} \left| \frac{\langle n_2 | e^{ik\hat{x}} | n_e \rangle \langle n_e | e^{ik\hat{x}} | n_1 \rangle}{\Delta + \nu(n_1 - n_e) - i\Gamma/2} \right|^2. \quad (28)$$

This rate describes two processes. The first term in the numerator  $|\langle n_2 | e^{ik\hat{x}} | n_e \rangle|^2$  describes the process of recoil due to spontaneous emission. The rest of the expression gives the rate of absorption and recoil from photons from the cooling light. Together, these two terms give the total rate of photon absorption and emission into motional states.

In the LD regime, the allowed motional state transition rates are

$$\gamma_{n \rightarrow n+1} = \eta^2 (n+1) A_+ \quad (29)$$

$$\gamma_{n \rightarrow n-1} = \eta^2 (n) A_- \quad (30)$$

where  $A_+$  and  $A_-$  are

$$A_+ = R(\Delta - \nu) + \alpha R(\Delta) \quad (31)$$

$$A_- = R(\Delta + \nu) + \alpha R(\Delta). \quad (32)$$

The function  $R(\Delta)$  is the low-saturation two-level system scattering rate

$$R(\Delta) = \Gamma \frac{\Omega^2/4}{\Delta^2 + (\Gamma/2)^2}. \quad (33)$$

The constant  $\alpha$  is related to the averaging over emission directions. Assuming emission into 1D gives  $\alpha = 1$ , but

averaging over emission into all directions leads to  $\alpha = 1/3$  [40].

In the LD regime, transfer only occurs between neighboring states, in which case the rate equation from Eq. 23 is

$$\begin{aligned} \dot{P}(n) = & \eta^2 A_- (n+1) P(n+1) + \eta^2 A_+ n P(n-1) \\ & - \eta^2 A_+ (n+1) P(n) - \eta^2 A_- n P(n). \end{aligned} \quad (34)$$

The cooling laser (Fig. 2(b), blue) drives the  $n+1$  and  $n-1$  sidebands with effective Rabi frequencies  $\Omega\eta\sqrt{n+1}$  and  $\Omega\eta\sqrt{n}$ . Decay (Fig. 2(b), red) of excited state to sideband occurs with probability  $\Gamma\eta^2 n$ .

Because the population only transfers between neighboring  $n$  in the LD regime, we can calculate the steady-state population by assuming no flow between two states:  $P(n+1)\gamma_{n+1 \rightarrow n} = P(n)\gamma_{n \rightarrow n+1}$ . Solving this equation leads to the steady-state condition

$$\frac{P(n+1)}{P(n)} = \frac{A_+}{A_-}. \quad (35)$$

We can set this equal to the Boltzmann factor to get the steady-state temperature:

$$\frac{P(n+1)}{P(n)} = \exp(-\hbar\nu/k_B T).$$

This represents a geometric distribution. Defining this ratio as  $s$ , the normalized solution is  $P(n) = (1-s)s^n$ , and the expectation and variance of  $n$  is  $\langle n \rangle = \frac{s}{1-s}$  and  $\langle (\Delta n)^2 \rangle = \frac{s}{(1-s)^2}$ .

Multiplying by  $n$  and summing over  $n$  gives the time rate equation for  $\langle n \rangle$ :

$$\frac{d\langle n \rangle}{dt} = \eta^2 [A_+ (\langle n \rangle + 1) - A_- \langle n \rangle] \quad (36)$$

The cooling rate is  $W_A = \eta^2(A_- - A_+)$ , which is balanced by the constant heating from spontaneous emission  $\eta^2 A_+$ . The steady-state solution is

$$\langle n \rangle = \frac{A_+}{A_- - A_+} = \frac{R(\Delta - \nu) + \alpha R(\Delta)}{R(\Delta + \nu) - R(\Delta - \nu)}. \quad (37)$$

In the resolved-sideband regime ( $\Gamma \ll \nu$ ), the lowest temperature occurs at the cooling sideband  $\Delta = -\nu$ , at which the steady-state is

$$\langle n \rangle = \frac{1}{4} \left( \frac{\Gamma}{\nu} \right)^2 \left( \alpha + \frac{1}{4} \right). \quad (38)$$

In the unresolved-sideband regime ( $\Gamma \gg \nu$ ), the steady state is [30, 36]

$$\langle n \rangle = \frac{(1 + \alpha)}{8} \left( \frac{\Gamma}{2\Delta} + \frac{2\Delta}{\Gamma} \right) - \frac{1}{2}. \quad (39)$$

In Fig. 2 we simulate the exact solution using the master equation from Eq. 3. Fig. 2(c-d) are in the unresolved and resolved sideband regimes for  $\eta = 0.05$  and in the low power limit  $\Omega = 0.05/\Gamma$ . In the resolved regime in (d), best cooling occurs at  $\Delta = -\nu$  and agrees closely with Eq. 38. The unresolved regime in (e) is a zoomed plot of the lower left corner of (d). Theoretically, the lowest temperature occurs for  $\Delta = -\Gamma/2$ , although the exact solution shows that it is broad and not much better than the resolved criteria  $\Delta = -\Gamma$ .

In plot Fig. 2(e), we plot steady-state population versus the trapping frequency for various LD parameters  $\eta$ . The population converges for  $\eta < 0.1$ .

The cooling performance of sideband cooling can be improved by adding a second counter-propagating beam with the same polarization to form a standing wave and placing the atom at the node of the field [43]. Although the atom now sees zero intensity at the equilibrium position, the sidebands are still driven. This can be seen by expanding the atom-field interaction as a series to first order in terms of the LD parameter and field gradient

$$H_I = -\frac{\Omega}{2} \left[ \left( \epsilon(0) + \hat{x} \frac{d\epsilon(0)}{d\hat{x}} \right) \cdot \mathbf{D}^\dagger + h.c. \right]. \quad (40)$$

The gradient can be either a phase or amplitude gradient, both of which drive the sideband. Intensity at the position of the atom does not lead to cooling and, in fact, only leads to extra heating. If we place the atom in a standing wave with linear polarization, the field is  $\epsilon(\hat{x}) = \sin(k\hat{x})$ . Fig. 2(f) simulates the steady-state population versus atom position with  $\nu = -\Delta$ . Theoretically, this gets rid of the process in Fig. 2(b) of driving  $n$  to  $n$ , followed by spontaneous emission heating to

the sideband. The steady-state solution is the same except with  $\alpha = 0$ . Cooling can be further enhanced by placing the atom in a cavity that can enhance the red sideband [44, 45].

### A. Excited state with different trapping frequency

The Doppler cooling section assumed that the electronic ground and excited states have the same trapping frequency. But typically, the ground and excited states of neutral atoms have different polarizabilities except at “magic wavelengths.” The different potentials lead to heating due to the abruptly changing dipole force during absorption or emission, shown in the schematics in Fig. 3. In the extreme case, the excited state is anti-trapped resulting in loss of the atom if the excited lifetime is long compared to  $1/\nu$ .

Because magic wavelengths are not often convenient for optical trapping, neutral atoms more often use two-photon cooling schemes, such as polarization gradient cooling and Raman sideband cooling. However, alkaline-earth atoms contain narrow linewidth transitions that have been used for imaging and cooling [10, 46], even ground-state cooling in Ref. [47]. Alkali atoms also contain narrow lines from forbidden transitions like the quadrupole transition of the S to D transition [48] or (n)S to (n+1)P transitions [49].

While sideband cooling with different trapping frequencies has been investigated through simulations [50], in this section we derive a novel analytical formula for capturing the effects of different trapping frequencies, which also demonstrates additional opportunities for cooling on higher order sidebands.

We now derive the equations for an atom with a ground-state frequency  $\nu$  and an excited state frequency  $\nu_e$ . The excited state harmonic eigenstates are stretched or compressed relative to the ground-state eigenstates. The squeezing operator from quantum optics can therefore be utilized to relate the wavefunctions in the two potentials: [51–53]

$$|m_e\rangle = \hat{S}^\dagger(r) |n_e\rangle, \quad (41)$$

where  $|n_e\rangle$  is the ground-state basis  $|m_e\rangle$  is the excited state basis. The squeezing operator  $\hat{S}(r)$  is

$$\hat{S}(r) = \exp\left(\frac{r}{2}(\hat{a}^2 - \hat{a}^{\dagger 2})\right). \quad (42)$$

The squeezing parameter  $r$  is related to the trapping frequencies by

$$r = \frac{1}{2} \ln\left(\frac{\nu_e}{\nu}\right). \quad (43)$$

The excited state annihilation operator is related to the ground-state annihilation operator by

$$\hat{a}_e = \hat{S}^\dagger(r) \hat{a} \hat{S}(r). \quad (44)$$

The harmonic Hamiltonian is

$$\begin{aligned} H_h &= \nu(\hat{a}^\dagger \hat{a})P_g + \nu_e(\hat{a}_e^\dagger \hat{a}_e)P_e \\ &= \nu(\hat{a}^\dagger \hat{a})P_g + \nu_e \hat{S}^\dagger(r)(\hat{a}^\dagger \hat{a})\hat{S}(r) P_e. \end{aligned} \quad (45)$$

The transfer rates between the ground-states are similar to Eq. 27, where now the squeezing operators are used to modify the excited harmonic states:

$$\begin{aligned} \gamma_{n_1 \rightarrow n_2} &= \Gamma \Omega^2 \\ &\times \sum_{\pm} \left| \sum_{n_e} \frac{\langle n_2 | e^{\pm ik\hat{x}} \hat{S}^\dagger(r) | n_e \rangle \langle n_e | \hat{S}(r) e^{ik\hat{x}} | n_1 \rangle}{(\Delta + \nu n_1 - \nu_e n_e) - i\Gamma/2} \right|^2. \end{aligned} \quad (46)$$

The sum over the excited states cannot generally be taken out of the magnitude now because each term does not necessarily have the directional emission terms. The transition matrix elements now contain the squeezing operator. To first order in  $r$  and  $\eta$ , the matrix elements are

$$\begin{aligned} &\langle n_e | \hat{S}(r) e^{ik\hat{x}} | n_1 \rangle \\ &= \langle n_e | \left( 1 + i\eta(\hat{a} + \hat{a}^\dagger) + \frac{r}{2}(\hat{a}^2 - (\hat{a}^\dagger)^2) \right) | n_1 \rangle. \end{aligned} \quad (47)$$

The first order LD terms couple  $n \rightarrow n \pm 1$ . In contrast, the first-order squeezing terms couple  $n \rightarrow n \pm 2$ , preserving the symmetry of the wavefunction.

The resonance condition for the light absorption is now determined by the detuning  $\Delta + \nu n_1 - \nu_e n_e$ , which we can re-express in terms of the difference trapping frequency can be rewritten as  $\Delta + \nu n_1 - \nu_e n_e = (\Delta + n_e \Delta\nu) + \nu(\nu_1 - \nu_e)$ , where the trapping frequency difference is  $\Delta\nu = \nu_e - \nu$ . For increasing  $n$ , the detuning between  $n_1 = n_e$  changes by  $\nu n$ . We define the resonance condition for the  $n$ 'th harmonic state as

$$\Delta_n = \Delta + n \Delta\nu. \quad (48)$$

The  $n \rightarrow n \pm 1$  transition are similar to before

$$\gamma_{n \rightarrow n+1} = \eta^2 (n+1) A_+ \quad (49)$$

$$\gamma_{n \rightarrow n-1} = \eta^2 n A_-. \quad (50)$$

The rates are a function of the  $n$  dependent detunings

$$A_+ = R(\Delta_n - \nu) + \alpha R(\Delta_n) \quad (51)$$

$$A_- = R(\Delta_n + \nu) + \alpha R(\Delta_n). \quad (52)$$

In this context, the rates add incoherently due to the randomized phase acquired during emission in multiple directions. As illustrated in Fig. 3(a), the  $n$ -dependent detuning results in the first-order cooling sideband being resonant only for a specific vibrational quantum number  $n$ . For a less tightly trapped excited state (left panel), the cooling light shifts towards heating sidebands for higher  $n$  values. Conversely, lower  $n$  values gradually shift towards cooling of higher-order sidebands. This effect leads to instability when  $\nu_e/\nu < 1$ , where higher-energy populations heat out of the trap. When  $\nu_e/\nu > 1$ , a type

of ‘‘cap’’ emerges, with heating occurring below a certain  $n$  value and cooling above it. Consequently, this cap effectively traps population below it.

The squeezing operator now also allows  $n \rightarrow n \pm 2$  transitions to first order in  $r$ :

$$\gamma_{n \rightarrow n+2} = r^2 (n+2)(n+1) B_+ \quad (53)$$

$$\gamma_{n \rightarrow n-2} = r^2 n(n-1) B_-. \quad (54)$$

The new rates  $B$  are a sum over different excited states, but the coherence/interference now matters because the coupling does not involve spontaneous emission to first order,

$$B_- = |T(\Delta_n) - T(\Delta_n + 2\nu)|^2 \quad (55)$$

$$B_+ = |T(\Delta_n) - T(\Delta_n - 2\nu)|^2. \quad (56)$$

The complex scattering rates are

$$T(\Delta) = \sqrt{\Gamma} \frac{\Omega/2}{\Delta - i\Gamma/2}. \quad (57)$$

and are related to the  $R$  rates by  $|T(\Delta)|^2 = R(\Delta)$ . Interestingly, the destructive interference between the two excited pathways in the  $n \rightarrow n \pm 2$  transition results in a transfer rate that cancels for large detuning, leading to much lower heating rates at large detuning.

Next we estimate the final temperature as a function of  $\Delta\nu$ . We construct a rate equation for  $\langle n \rangle$  by multiplying the rate equation in Eq. 23 by  $n$  and summing over all  $n$ . This leads to the rate equation

$$\begin{aligned} \frac{d\langle n \rangle}{dt} &= \eta^2 [A_+ (\langle n \rangle + 1) - A_- \langle n \rangle] \\ &+ 2r^2 [B_+ (\langle n \rangle + 2)(\langle n \rangle + 1) - B_- \langle n \rangle (\langle n \rangle - 1)]. \end{aligned} \quad (58)$$

Although we would need a separate expression for  $\langle n^2 \rangle$  to solve this exactly, we can find an approximate solution by assuming the population follows a geometric series with a Boltzmann factor, as was the case in the Doppler section. Then we can use the property  $\langle n^2 \rangle = 2\langle n \rangle^2 + \langle n \rangle$  for geometric distributions and solve the equation numerically to estimate the steady-state  $\langle n \rangle$ , which gives the equation

$$\begin{aligned} 0 &= \eta^2 [\langle n \rangle (A_+ - A_-) + A_+] \\ &+ 4r^2 [\langle n \rangle^2 (B_+ - B_-) + B_+ (2\langle n \rangle + 1)]. \end{aligned} \quad (59)$$

$B_{\pm}$  and  $A_{\pm}$  are also  $n$  dependent through the detuning  $\Delta_n$ . This solution agrees well for small  $r$  and  $\eta$ , with the main assumption that the distribution follows a geometric series. This will break down for high populations as the cooling and heating become  $n$  dependent.

Cooling is a balance between the sideband and squeezing terms. Cooling due to sidebands is  $W_A \approx \eta^2 (A_- - A_+)$ , while squeezing cooling is  $W_B \approx 2r^2 (B_- - B_+)$ , with the squeezing dependence being quadratic. Additionally, there is heating from both that goes as  $\eta^2 A_+$



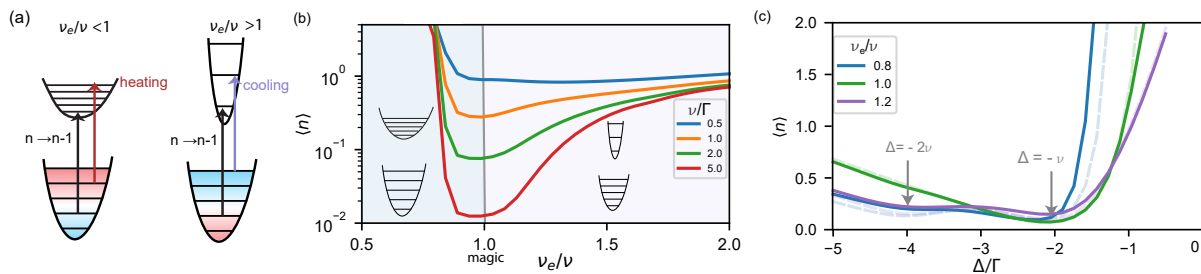


FIG. 3. Sideband cooling with different trapping frequencies. **(a)** Two regimes, where the excited state is less trapped (left) or more trapped (right) result in extra heating. This heating comes from coupling many different motional states in the quantum picture, or a fluctuating dipole force in the classical picture. For different trapping frequencies, the  $n$  to  $n - 1$  transition can be resonant for only one specific  $n$ . For  $\nu_e < \nu$ , higher  $n$  gradually shift more blue towards heating. For  $\nu_e > \nu$ , higher  $n$  gradually shifts more red, leading to cooling of higher order sidebands. **(b)** Population for a different excited state trapping frequency  $\nu_e$ , plotted for different  $\nu/\Gamma$  and  $\eta = 0.1$  and  $\Delta = -\nu$ . The magic condition is  $\nu_e/\nu = 1$ . **(c)** Population versus detuning for different excited to ground trapping frequency ratios  $\nu_e/\nu$ . A minimum occurs at  $\Delta = -\nu$ , but a second minimum occurs at  $\Delta = -2\nu$  when  $\nu_e \neq \nu$ . Plot is for  $\eta = 0.1$ ,  $\nu/\Gamma = 2$ . Eq. 59 is plotted in a light dashed line. Different trapping frequencies allow the coupling of higher order sidebands, providing new opportunities for cooling.

and  $2r^2B_+$ , respectively. Interestingly, the squeezing results in a coupling between different motional states and can be used for cooling, as shown below.

Fig. 3(b) is a master equation simulation of steady-state population versus the excited to ground-state trapping frequency ratio  $\nu_e/\nu$ . The magic condition is  $\nu_e/\nu = 1$ . Cooling performance drops on both sides, with much more dramatic for a weaker excited state ( $\nu_e/\nu < 1$ ). Fig. 3(c) is a detuning scan for  $\eta = 0.1$ ,  $\nu = 2\Gamma$ , and various  $\nu_e/\nu$ . There is a resonance at  $\Delta = -\nu$  due to sideband cooling, but also a second resonance at  $\Delta = -2\nu$  due to the squeezing coupling.

For cooling the atom in a ‘non-magic’ trap, a technique known as ‘Sisyphus Cooling’, has been recently demonstrated in tweezers [54, 55]. In situations where the polarizability of the excited state is greater (or less) than that of the ground-state, the atom experiences a deeper (or shallower) trap upon excitation by the cooling laser. This difference enables the implementation of ‘attractive’ (or ‘repulsive’) Sisyphus cooling. In the repulsive Sisyphus cooling method, there is a limit known as the Sisyphus cap to how much the atom can be cooled. However, in the attractive Sisyphus regime, significantly lower temperatures can be achieved within the trap. Ref. [50] proposes that sweeping the cooling laser’s frequency adiabatically could achieve temperatures well below the Sisyphus cap.

#### IV. SUB-DOPPLER COOLING WITH SPIN

Doppler cooling alone is often insufficient for achieving ground-state cooling of neutral atoms in optical traps due to two main issues. First, the trapping frequencies in optical traps are typically less than 100 kHz, while the line widths of the D1 and D2 transitions are around 5 MHz, placing them far into the unresolved regime. Second, the ground and excited states have different optical polarizabilities, which can lead to additional heating and atom

loss due to far-off-resonant trapping light.

To overcome these limitations, sub-Doppler cooling schemes such as polarization gradient (PG) [13], gray molasses (GM) and  $\Lambda$ -enhanced GM [17, 18], electromagnetically induced transparency (EIT) cooling [56], and Raman sideband (RSB) [27] employ two-photon transitions between ground-states, as illustrated in Fig. 4(a). By detuning the cooling laser far from the excited states, these techniques mitigate the issues associated with the unresolved regime and differential polarizabilities. Furthermore, the ground hyperfine states in neutral atoms generally experience the same light shifts, resulting in similar trapping frequencies for different spin states.

Two-photon cooling schemes rely on coupling two spin states with different motional quantum numbers,  $n$ , and energies. The quantum model for PG and GM cooling is depicted in Fig. 4(d,f). In the first stage, a two-photon coherent transition (green) changes the spin and motional states, where the motional state decreases from  $n$  to  $n - 1$ . In the second stage, spontaneous emission (red) from the cooling light or a separate beam then re-pumps the atom back to the original spin state, allowing the cooling cycle to repeat. As long as the trapping frequency energy,  $\hbar\nu$  is larger than the recoil energy,  $E_{\text{recoil}}$ , net cooling can be achieved, as the average heating from spontaneous emission is limited to one photon recoil.

In this section, we present a unified spin cooling formalism that encompasses PG, GM, EIT,  $\Lambda$ -GM, and RSB cooling. We show that all these schemes exhibit similar forms of the effective Hamiltonian and collapse operators in the LD regime and rely on the same principles. PG and GM cooling use a single counter-propagating laser frequency to create light shifts similar to the trapping frequency, as well as the Raman coupling and optical pumping. EIT and  $\Lambda$ -GM cooling incorporate a second coherent laser to address other spin states and exploit the dark states of a three-level  $\Lambda$  system to create darker reservoir states. RSB cooling separates all three pro-

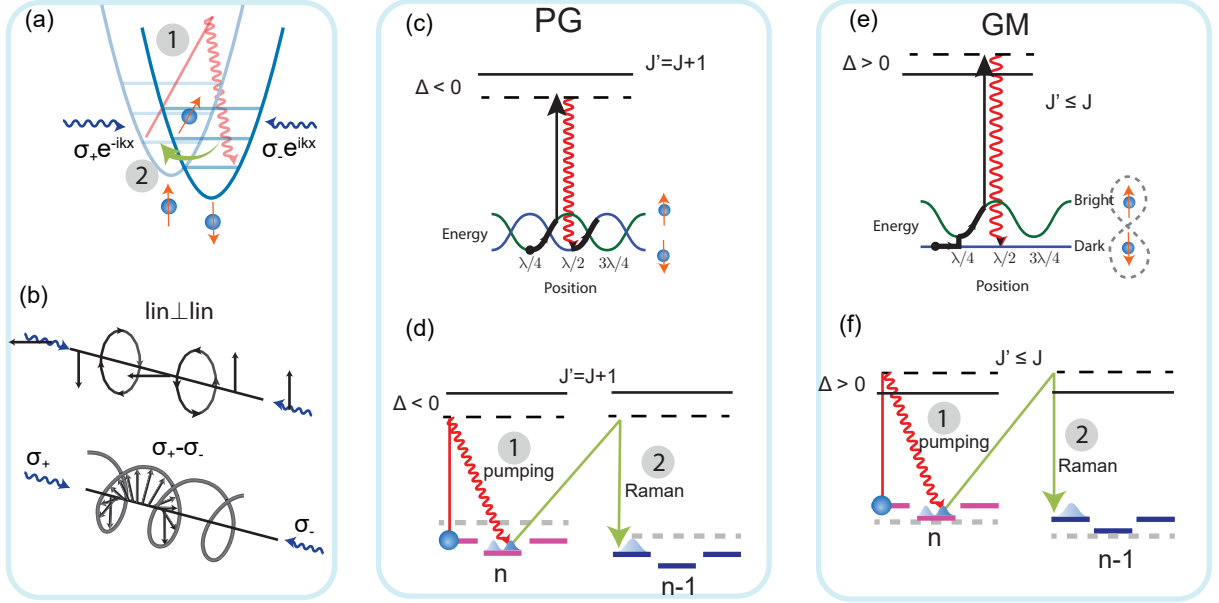


FIG. 4. Spin cooling. (a) An atom with spin in a harmonic trap with changing polarization. (b)  $\text{lin} \perp \text{lin}$  and  $\sigma_+ - \sigma_-$  polarization. (c-d) Free-space (top) and quantum picture (bottom) for PG cooling, which uses  $F \rightarrow F + 1$  and red detuning. Population is optically pumped into the lower energy state. (e-f) Free-space (top) and quantum picture (bottom) for GM cooling, which uses  $F' \leq F$  and blue-detuning to create dark states, which act as the lower energy state into which the population is pumped.

cesses, using two lasers to couple different ground spin states and a third frequency and beam for optical pumping that uses angular momentum selection rules to keep the cooling state dark.

### A. Polarization Gradient Cooling and Gray Molasses

PG cooling was described theoretically by Cohen-Tannoudji in the late 1980's [13] and resulted in sub-doppler temperatures in the first magneto-optical traps [57]. Two different PG models were presented in free space for the case of  $\text{lin} \perp \text{lin}$  and  $\sigma_+ - \sigma_-$  polarizations, shown in Fig. 4(b). The  $\text{lin} \perp \text{lin}$  configuration comes from counter-propagating orthogonal linear polarization beams, resulting in a polarization that changes from linear to circular. This model works on a  $F = 1/2$  to  $F' = 3/2$  atom, and the free-space picture is shown in Fig. 4(c). The circular polarization results in a vector shift  $\Delta E \propto m_J$  that modulates every wavelength. PG cooling works by having an optical pumping that pumps the atom to the lower potential. As the atom travels, it goes up the potential hill, loses energy, and then is pumped back to the bottom. The cycle repeats until the atom reaches the recoil temperature  $E_{\text{recoil}}$ , which is typically a few  $\mu\text{K}$ . This style of cooling is also called Sisyphus cooling, named after the Greek mythological figure who was condemned to eternally push a boulder up a hill.

The  $\sigma_+ - \sigma_-$  model is applicable when counter-propagating laser beams with opposite circular polariza-

tions are used. As shown in Fig. 4(b), the resulting polarization is linear at every point in space but rotates along the propagation direction with a period equal to the wavelength. The  $\sigma_+ - \sigma_-$  model relies on the tensor shift and therefore requires a ground-state spin of at least  $F = 1$ . This version is more common because it is also the polarization configuration used by a magneto-optical trap (MOT).

Both forms of PG cooling work by using red-detuned light with a  $J \rightarrow J + 1$  transition, which is the same configuration used by a MOT for its stretch state cycling condition.

Gray Molasses (GM) is a closely related cooling scheme that operates with blue-detuned light with a  $F \rightarrow F$  or  $F \rightarrow F - 1$  transition. GM has achieved even colder temperatures than PG cooling [17, 58, 59] by storing cold atoms in dark states that do not interact with the cooling light due to polarization and angular momentum selection rules. For example in Fig. 4(e), certain ground-states are not coupled to the excited states. GM works with blue detuned light so that the bright states are higher in energy. Atoms that fall into these dark states are effectively shelved, reducing their interaction with the cooling light. The residual velocity couples the atom back into a bright state, where they can undergo Sisyphus cooling again.

However, these free-space models break down for a trapped atom in the Lamb-Dicke (LD) regime, where the atom's wavefunction is smaller than the cooling wavelength. While PG and GM have been implemented for atoms in optical lattices, tweezers [21, 60, 61], and

ions [62], they have not been described theoretically. The most related works have been Wineland et al. in Ref. [33], which studied a bound atom trapped in a linearly polarized standing wave, and Cirac et al. in Ref. [32] which investigated a  $J = 1/2 \rightarrow J' = 3/2$  atom in the lin $\perp$ lin configuration. Both of these studies found a lower limit for the mean vibrational quantum number,  $\langle n \rangle \approx 1$ . Here we develop a generalized spin cooling model that applies to all spins and polarizations and shows that certain configurations can lead to ground-state cooling.

## B. Spin cooling theory

First we look at the case of two counter-propagating beams with opposite-handed circular polarized light ( $\sigma_+$ - $\sigma_-$ ). The complex polarization is

$$\begin{aligned} \epsilon_{\sigma_+ - \sigma_-}(\hat{z}) &= \frac{i}{\sqrt{2}} (e^{ik\hat{z}} \hat{e}_1 + e^{-ik\hat{z}} \hat{e}_{-1}) \\ &= \sin(k\hat{z}) \hat{x} + \cos(k\hat{z}) \hat{y} \\ &\approx \hat{y} + (k\hat{z}) \hat{x} \end{aligned} \quad (60)$$

where  $\hat{e}_{1,0,-1}$  are the spherical unit vectors  $\hat{e}_{\pm 1} = \mp \frac{1}{\sqrt{2}}(\hat{e}_x \pm i\hat{e}_y)$  and  $\hat{e}_0 = \hat{e}_z$ , and also The field is Taylor expanded in the last line. A fixed atom sees only linear light. The intensity is constant everywhere. The polarization is linear but rotates every wavelength, as shown in Fig. 4(b). As it oscillates back and forth in the trap, it sees a small rotation of the field. For convenience, we choose the quantization axis  $\hat{z}$  to be aligned with linear polarization at equilibrium. The cooling is however independent of the atom position because the light is linear everywhere.

The Hamiltonian and collapse operator in the LD regime are

$$H_{\sigma_+ - \sigma_-} = \nu \hat{a}^\dagger \hat{a} + (\Delta - i\Gamma/2) P_e + \frac{\Omega}{\sqrt{2}} \left[ \hat{D}_z^\dagger - i\eta(\hat{a} + \hat{a}^\dagger) \hat{D}_x^\dagger + h.c. \right] \quad (61)$$

$$\hat{L}_{q,\pm} = \sqrt{\Gamma} (1 \pm ik\hat{x}) \hat{D}_q \quad (62)$$

The Cartesian dipole operators are defined as  $D_i = \hat{i} \cdot \hat{D}$ .

The PG cooling processes are illustrated in Fig. 4(d) for a  $F = 1$  atom. The position-independent interaction  $\hat{D}_z$  leads to a tensor shift and optical pumping. For the case of  $F = 1$  ground-state, the population is pumped (red) to the  $m = 0$  state. The position-dependent term in the interaction  $\eta(\hat{a} + \hat{a}^\dagger) \hat{D}_x$  drives an orthogonal polarization transition  $m \rightarrow m \pm 1$  while also changing the motional state. This drive is reduced by the LD parameter and produces heating due to spontaneous emission.

The last ingredient for cooling is a two-photon coherent Raman transition (green). One branch of this transition comes from the position-independent term, while the other branch comes from the position-dependent term. As shown in the illustration, together these terms produce a coherent transition from  $|m = 0, n\rangle$  to  $|m =$

$\pm 1, n - 1\rangle$ . As drawn, the resonance for this two-photon condition is satisfied when the differential light shift between the  $m = 0$  and  $m = \pm 1$  states are equal to the trapping frequency. This process then repeats, cooling the atom.

These processes can be seen more clearly by looking at the effective ground-state operators from Eq. 20. The effective ground-state Hamiltonian is

$$H_{\sigma_+ - \sigma_-}^{\text{eff}} = \nu \hat{a}^\dagger \hat{a} - \quad (63)$$

$$\frac{\Omega^2}{4\Delta} \left[ \hat{D}_z \hat{D}_z^\dagger + k\hat{x}(\hat{D}_z \hat{D}_x^\dagger + \hat{D}_x \hat{D}_z^\dagger) \right].$$

Converting it to spin operators using Eq. 19 gives an effective spin model

$$\begin{aligned} H_{\sigma_+ - \sigma_-}^{\text{eff}} &= \nu \hat{a}^\dagger \hat{a} + \frac{\Omega^2}{\Delta} \left[ C^{(0)} + C^{(2)}(\hat{F}_z^2 - \hat{F}^2/3) \right] \\ &+ k\hat{x} \frac{\Omega^2}{\Delta} C^{(2)} (\hat{F}_x \hat{F}_z + \hat{F}_z \hat{F}_x). \end{aligned} \quad (64)$$

The collapse operators are

$$L_{q,\pm}^{\text{eff}} = \sqrt{\Gamma} \frac{\Omega/2}{\Delta - i\Gamma/2} \left[ \hat{D}_q (\hat{D}_z^\dagger + ik\hat{x}(\hat{D}_z^\dagger + \hat{D}_x^\dagger)) \right]. \quad (65)$$

A spin version of this operator can also be found using Eq. 21.

This spin Hamiltonian is valid for all ground and excited spin combinations. While the ground-state spin determines the spin operators  $F_i$ , the excited state spin only affects the  $C^{(i)}$  coefficients. The Hamiltonian and collapse operator both have a position-independent and position-dependent term.

This expansion can be performed for other polarizations as well to get a similar form. We can also look at the lin $\perp$ lin case, where the polarization changes from circular to linear depending on the atom position,

$$\epsilon_{\text{lin}\perp\text{lin}}(\hat{x}, \phi) = \frac{1}{2} (e^{ik\hat{x}} \hat{x} + e^{i\phi} e^{-ik\hat{x}} \hat{y}). \quad (66)$$

For circular polarization, the interaction is

$$H_{\text{lin}\perp\text{lin}}^I(\phi = \pi/2) = \frac{\Omega}{2} \left[ \hat{D}_1^\dagger + \eta(\hat{a} + \hat{a}^\dagger) \hat{D}_{-1}^\dagger + h.c. \right], \quad (67)$$

and for linear polarization,

$$H_{\text{lin}\perp\text{lin}}^I(\phi = 0) = \frac{\Omega}{2} \left[ \hat{D}_z^\dagger + \eta(\hat{a} + \hat{a}^\dagger) \hat{D}_x^\dagger + h.c. \right]. \quad (68)$$

Before performing the full master equation simulations, our next goal is to develop a simple analytical model for a system with a Hamiltonian and collapse operator in these forms.

We derive an approximate temperature for a simplified model that captures both regimes. We use two spin states  $|\downarrow, n\rangle$  and  $|\uparrow, n\rangle$  and an effective Hamiltonian and collapse operators

$$\begin{aligned} H &= \nu \hat{a}^\dagger \hat{a} + V_0(\hat{F}_z + 1/2) + \Omega_R k \hat{x} \hat{F}_x \\ L_1 &= \sqrt{\gamma_+} (\hat{F}_+ + ik\hat{x} \hat{F}_x) \\ L_{-1} &= \sqrt{\gamma_-} (\hat{F}_- + ik\hat{x} \hat{F}_x). \end{aligned} \quad (69)$$

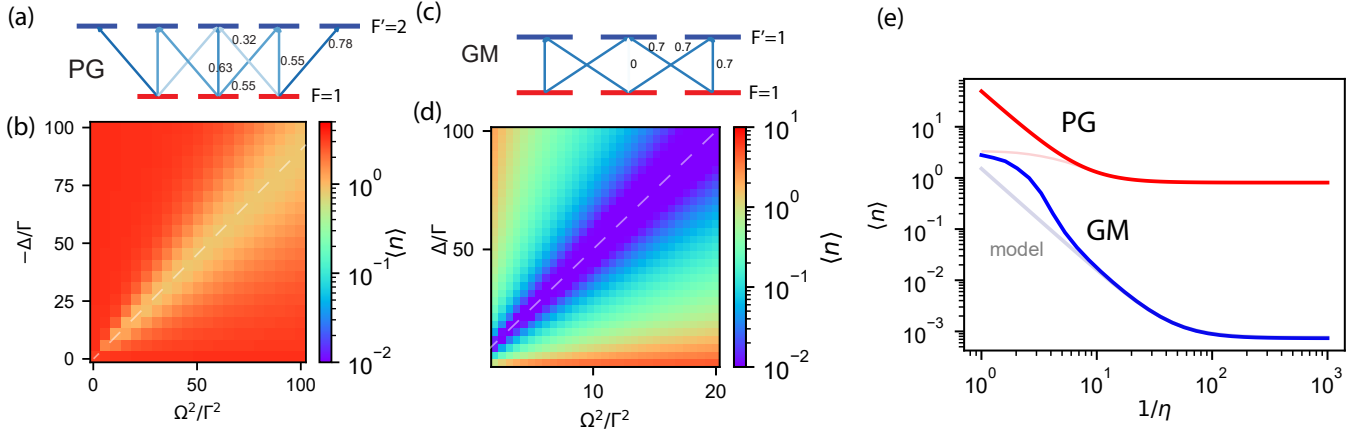


FIG. 5. PG and GM simulations. **(a-b)** Clebsch-Gordon coefficients for PG ( $F = 1$  to  $F' = 1$ ) and GM ( $F = 1$  to  $F' = 2$ ). For PG in linear light, the population pumps to the  $m = 0$  state, which is also the brightest state. PG cooling requires red-detuned light ( $\Delta < 0$ ). For GM in linear light, the population pumps to  $m = 0$  which is dark. GM cooling requires blue-detuned light ( $\Delta > 0$ ). **(c-d)** Simulations of  $\langle n \rangle$  versus cooling power for PG and GM. Optimal cooling occurs on a line (light-dashed) where the differential light shift equals the trapping frequency. PG is limited to  $\langle n \rangle \approx 1$ , while GM cools close to the ground-state due to the dark state. Simulations use  $\eta = 0.05$  and 8 harmonic states. **(e)** Optimal cooling for PG and GM versus the Lamb-Dicke parameter  $\eta$ . Optimal cooling occurs when the differential light shift is equal to the trapping frequency and in the limit of large detuning. The simple model from Eq. 73 is plotted in a lighter color. For PG,  $\Delta = -20\Gamma$  and for GM  $\Delta = 20\Gamma$ . The optical cooling powers were adjusted to make the Raman transition resonant.

$V_0$  is a spin-dependent light shift. Position-independent collapse parts with pumping rates  $\gamma_+$  and  $\gamma_-$  are the optical pumping between the spin states. The  $\Omega_R k \hat{x} \hat{F}_x$  term produces Raman transitions between  $|\uparrow, n\rangle$  and  $|\downarrow, n-1\rangle$ .  $\Omega_R = \Omega^2/\Delta C^{(2)}$ . The optimal light shift for cooling is to make these two states the same frequency by setting  $V_0 = \nu$ . The  $|\downarrow, n\rangle$  couples to  $|\uparrow, n-1\rangle$ , but off-resonantly so we can ignore it.

To find an approximate expression for the steady-state temperature, we first use the master equation to determine the steady-state coherences between the Raman-coupled states:

$$\langle \uparrow, n | \rho | \downarrow, n-1 \rangle = \frac{i\sqrt{n}\eta\Omega_R}{\Delta - i(\gamma_- + \gamma_+)/2} [P_\uparrow(n) - P_\downarrow(n-1)] \quad (70)$$

By substituting this coherence into the density matrix equations and ignoring off-resonance coherences, we obtain the transfer rate  $\Gamma_R$  between  $|\uparrow, n\rangle$  to  $|\downarrow, n-1\rangle$ :

$$\Gamma_R = \frac{4\eta^2\Omega_R^2}{(\gamma_+ + \gamma_-)} \frac{1}{1 + 4\Delta_r^2/(\gamma_+ + \gamma_-)^2}. \quad (71)$$

$\Delta_r$  is the relative detuning between the two states. Optimal cooling occurs when the light shifts bring these states into resonance, i.e.,  $\Delta_r = 0$ . Although there are off-resonant transitions, such as  $|n, \downarrow\rangle \rightarrow |n-1, \uparrow\rangle$ , we ignore them in this simple model. By neglecting all off-resonant

coherences, we arrive at the population rate equations:

$$\begin{aligned} \frac{dP_\downarrow(n)}{dt} &= \Gamma_R (n+1) [-P_\downarrow(n) + P_\uparrow(n+1)] \\ &\quad + \gamma_- P_\uparrow(n) - \gamma_+ P_\downarrow(n) \\ &\quad + \eta^2 \gamma_h [(n+1)P_\uparrow(n+1) + nP_\uparrow(n-1) - (2n+1)P_\downarrow(n)] \\ \frac{dP_\uparrow(n)}{dt} &= n\Gamma_R [P_\downarrow(n-1) - P_\uparrow(n)] \\ &\quad - \gamma_- P_\uparrow(n) + \gamma_+ P_\downarrow(n) \\ &\quad + \eta^2 \gamma_h [(n+1)P_\downarrow(n+1) + nP_\downarrow(n-1) - (2n+1)P_\uparrow(n)] \end{aligned} \quad (72)$$

Here  $\gamma_h = \gamma_+ + \gamma_-$  is a scattering rate related to spontaneous emission heating. Next, we calculate the steady state solution for  $\langle n \rangle$ . The derivation is as follows. First, we sum the two equations in Eq. 72, yielding a single equation. Next, we multiply the distribution equations by  $n$  and sum from  $n = 0$  to  $\infty$ , resulting in two equations containing higher-order moments  $\langle n^2 \rangle_\downarrow$  and  $\langle n^2 \rangle_\uparrow$ .

In these four expressions, we have six unknowns:  $\langle n^2 \rangle_\uparrow$ ,  $\langle n^2 \rangle_\downarrow$ ,  $\langle n \rangle_\uparrow$ ,  $\langle n \rangle_\downarrow$ , and the fraction of population in either up or down  $P_\uparrow = \sum_{n=0} P_\uparrow(n)$ ,  $P_\downarrow = \sum_{n=0} P_\downarrow(n)$ . We make these equations solvable by simplifying the higher-order moments by assuming that both  $P_\uparrow(n)$  and  $P_\downarrow(n)$  follow a geometric distribution.

We can express  $\langle n^2 \rangle_\uparrow$  as  $\langle n^2 \rangle_\uparrow = 2\langle n \rangle_\uparrow / P_\uparrow + \langle n \rangle_\uparrow$ , where  $P_\uparrow$  and  $P_\downarrow$  appear because they are not a normalized distribution. Then we solve the system of equations for  $\langle n \rangle_\uparrow + \langle n \rangle_\downarrow = \langle n \rangle$ .

We then take the limit of large detuning to obtain a simpler analytical expression compared to the complete solution. In the large detuning limit, the cooling rate  $\Gamma_R = 4\Omega_R^2\eta^2/(\gamma_+ + \gamma_-)$  dominates. The cooling rate

$\Gamma_R$  is independent of detuning because both  $\Omega_R^2$  and the scattering rate scale as  $1/\Delta^2$ . Consequently, for large detuning,  $\Gamma_R$  becomes the dominant rate, and the population quickly distributes between the two Raman-coupled states. The asymmetry of the optical pumping then determines the cooling efficiency and the final temperature. In this limit of large detuning, the Raman coupling rate is faster than any scattering rate, and the population simplifies to

$$\langle n \rangle = \frac{s}{(1-s)}, \quad s = \frac{4\eta^2\gamma_h + \gamma_+}{\eta^2\gamma_h + \gamma_-}. \quad (73)$$

We note that a similar expression can also be derived from the no-flow condition solving for  $s = P(n+1)/P(n)$  without having to take the expectation values, although other approximations have to be made.

This analytical model is the final result of this model and provides intuition for the cooling performance of PG and GM. It agrees very well with the exact spin 1/2 solution for  $\eta < 0.1$ . For other spin models, it also serves as a fitting function. The ratio  $\gamma_+/\gamma_-$  is then an effective asymmetry of the optical pumping to the lower energy state. This asymmetry is close to unity for PG cooling, and much smaller for cooling with dark state, i.e. GM and  $\Lambda$ -GM. The ratio  $\gamma_h/\gamma_+$  is an effective scattering rate of the lower energy state. Together with the Lamb-Dicke parameter  $\eta$ , these three parameters determine the lowest achievable population.

In Fig. 5, we simulate the full master equation with ground and excited states for PG and GM for  $F = 1$  ground-state in  $\sigma_+ - \sigma_-$  light, meaning that the light is linear at the atom equilibrium position. The PG case is  $F = 1$  to  $F' = 1$ , and the Clebsch-Gordan (CG) coefficients are shown in (a). In the  $\sigma_+ - \sigma_-$  configuration, the  $m = 0$  state has the largest CG and, consequently, the largest Stark shift. In linear light, however, the population still pumps to the  $m = 0$  state because of strong diagonal CG coefficients from  $|J' = 2, m = \pm 1\rangle$ . Cooling requires that the population is pumped to the lowest energy state. Therefore, cooling requires the red-detuned configuration where the  $m = 0$ , which is the most stark shifted state, is also the lowest energy, as shown in Fig. 4(d).

In the PG simulation in Fig. 5(b), cooling is optimum along the line where the Raman transition is resonant. The optical power of the cooling light is such that the energy difference between  $m = 0$  and  $m = \pm 1$  equals the trapping frequency. The lowest population converges to  $\langle n \rangle = 0.9$  in the limit of large detuning  $\Delta$  and small LD parameter  $\eta$ . The optimal value is plotted in red in Fig. 5(e). The light red line is the simple model from Eq. 73 with pumping asymmetry  $\gamma_-/\gamma_+ = 0.45$ , and heating scattering  $\gamma_h/\gamma_+ = 27$ . There is not a large asymmetry in the optical pumping, and  $\gamma_+ \sim \gamma_-$ , which are both larger than  $\eta^2\gamma_s$  in the LD regime. In this case, the final population is  $s \approx \gamma_+/\gamma_-$ . In this situation, the cooling reaches a fundamental limit for large detuning and small  $\eta$ .

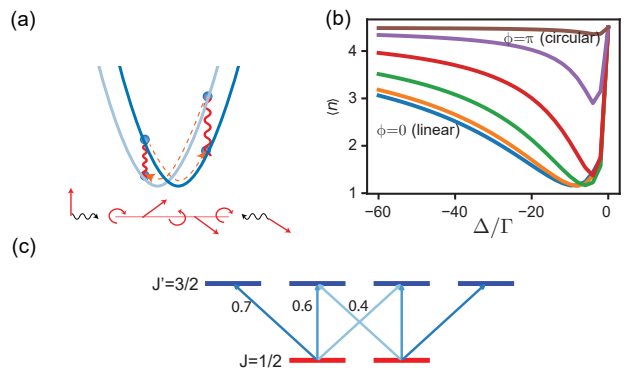


FIG. 6.  $J = 1/2$  to  $J' = 3/2$  PG cooling in lin $\perp$ lin light. (a) Classical picture of cooling with spins in polarization gradient of lin $\perp$ lin light, inspired from Ref. [32]. (b) Cooling for different atom positions, which corresponds to different polarizations. Best cooling occurs at linear light, and give  $\langle n \rangle \approx 1$ . (c) Clebsch-Gordan coefficients for  $J = 1/2$  to  $J' = 3/2$ .

Next we look at GM for  $F = 1$  to  $F' = 1$ . The CG coefficients are in Fig. 5(c). One optical selection rule is that the  $|F, m = 0\rangle$  to  $|F', m = 0\rangle$  is forbidden, due to the photon needing to add one unit of angular momentum. Because of this dark state, all the population pumps to  $m = 0$ . But in contrast to PG, this state is now dark. For that reason GM requires blue-detuned light ( $\Delta > 0$ ) to make this state the lowest energy. The simulation in Fig. 5(d) again shows that optimal cooling occurs when the light shift equals the trapping frequency. The population however drops close to ground-state. The optimal cooling is plotted in Fig. 5(e), along with the simple model with effective parameters  $\gamma_-/\gamma_+ = 7.5 \times 10^{-4}$  and heating scattering  $\gamma_h/\gamma_+ = 1.5$ . For this large optical pumping asymmetry where the reservoir state is dark, such as found in GM and EIT cooling,  $\gamma_- = 0$ , and  $s \approx \frac{\gamma_+}{\eta^2\gamma_h}$ . In this dark cooling limit, the final population is instead limited by  $\eta$ .

In Fig. 6, we also investigate the case of  $J = 1/2$  to  $J' = 3/2$  for lin $\perp$ lin, which was studied in Ref. [32]. There is no cooling for  $\sigma_+ - \sigma_-$ , which requires at least three ground spins due to the tensor shift. This configuration is not relevant for neutral atoms, but it is for ions. Because the polarization in lin $\perp$ lin changes with position, we plot the cooling as a function of atom position, with  $\phi = 0$  linear and  $\phi = \pi/2$  circular. Similar to the other PG model, the population converges to  $\langle n \rangle \approx 1$ . Interestingly though, this occurs for when the polarization is linear, not circular. This is because circular polarization cooling also requires three spins because the Raman transition supplies two angular momenta. The cooling still occurs for when the light shift is equal to the trapping frequency [32]. However, we do find that for larger spin states, circular polarization is the best cooling, in agreement with our model.

### C. $\Lambda$ -GM and EIT Cooling

The simple models reveal a crucial insight: lower populations are achieved when pumping to darker states. Gray molasses (GM) cooling generates dark states through angular momentum selection rules. Electromagnetically induced transparency (EIT) cooling and  $\Lambda$ -type gray molasses ( $\Lambda$ -GM) create additional dark states by incorporating multiple ground-states addressed with a second laser frequency in an EIT configuration, as illustrated in Fig. 7(a). These dark states arise from the interference of two lasers coupling the ground-states to a common excited state.

Historically, the term ‘‘EIT cooling’’ has been primarily associated with trapped ions [63, 64], where the two ground-states are typically different Zeeman sublevels. In contrast, ‘‘ $\Lambda$ -GM’’ is commonly used in the context of neutral atoms [20, 61], where the two ground-states belong to different hyperfine manifolds of the ground-state.

Cooling to the motional ground-state using EIT has been theoretically predicted and achieved experimentally in  $Ca^+$  ion using Zeeman sublevels of the D1 line [56, 63].  $\Lambda$ -enhanced GM cooling on the other hand is proven effective not only for bound atoms [21] but also for cooling and imaging molecules in optical traps [65].

EIT addresses two ground-states  $|g_1\rangle$  and  $|g_2\rangle$  with two different Rabi frequencies  $\Omega_1$  and  $\Omega_2$ . These two states are typically from different hyperfine ground-states. Each ground-state is addressed by a laser frequency to a single excited state with corresponding detunings  $\Delta_1$  and  $\Delta_2$ . The Hamiltonian is written with  $g_1$  in the rotating frame of laser one and  $g_2$  in the rotating frame of laser two,

$$H_0 = \nu a^\dagger a + \Delta_1 |g_1\rangle\langle g_1| + \Delta_2 |g_2\rangle\langle g_2|. \quad (74)$$

We have two dipole operators,  $\hat{D}_1 = |g_1\rangle\langle e|$  and  $\hat{D}_2 = |g_2\rangle\langle e|$ . The interaction Hamiltonian is

$$H_I = \frac{\Omega_1}{2} (\hat{D}_1^\dagger e^{ik_1 \hat{x}} + h.c.) + \frac{\Omega_2}{2} (\hat{D}_2^\dagger e^{ik_2 \hat{x}} + h.c.). \quad (75)$$

The two collapse operators represent the spontaneous emission of the single excited state to both ground-states,

$$L_{1,\pm} = \sqrt{\Gamma} e^{\pm ik_1 \hat{x}} \hat{D}_1, \quad L_{2,\pm} = \sqrt{\Gamma} e^{\pm ik_2 \hat{x}} \hat{D}_2. \quad (76)$$

Next, we perform a unitary transformation of the two ground-states into two superpositions so that only one of them is coupled to the two lasers, and the other is the EIT dark state, shown in Fig. 7(b). The dark state is dark due to the destructive interference of the population in the excited state from the two ground-states. The basis transformation is

$$\begin{aligned} |g_B\rangle &= \frac{1}{\Omega_{\text{rms}}} (\Omega_1 |g_1\rangle + \Omega_2 |g_2\rangle) \\ |g_D\rangle &= \frac{1}{\Omega_{\text{rms}}} (-\Omega_2 |g_1\rangle + \Omega_1 |g_2\rangle) \\ |e\rangle &= |e| \end{aligned} \quad (77)$$

where  $\Omega_{\text{rms}} = \sqrt{\Omega_1^2 + \Omega_2^2}$ .

Under this transformation, the bare Hamiltonian is

$$\begin{aligned} H_0 &= \nu a^\dagger a + \Delta_B |g_B\rangle\langle g_B| + \Delta_D |g_D\rangle\langle g_D| \\ &\quad + \Omega_{BD} (|g_B\rangle\langle g_D| + |g_D\rangle\langle g_B|), \end{aligned} \quad (78)$$

with the energies of the bright and dark states as

$$\begin{aligned} \Delta_B &= (\Omega_1^2 \Delta_1 + \Omega_2^2 \Delta_2) / \Omega_{\text{rms}}^2 \\ \Delta_D &= (\Omega_1^2 \Delta_2 + \Omega_2^2 \Delta_1) / \Omega_{\text{rms}}^2, \end{aligned} \quad (79)$$

and a coupling between the dark and bright states

$$\Omega_{BD} = (\Delta_2 - \Delta_1) \frac{\Omega_1 \Omega_2}{\Omega_1^2 + \Omega_2^2}. \quad (80)$$

The transformed atom-field interaction is

$$\begin{aligned} H_I &= \frac{1}{2\Omega_{\text{rms}}} \left[ D_B^\dagger (\Omega_1^2 e^{ik_1 \hat{x}} + \Omega_2^2 e^{ik_2 \hat{x}}) \right. \\ &\quad \left. + D_D^\dagger \Omega_1 \Omega_2 (e^{ik_1 \hat{x}} - e^{ik_2 \hat{x}}) + h.c. \right]. \end{aligned} \quad (81)$$

In the case where the two lasers are two-photon resonant, the Rabi frequencies are equal  $\Omega_1 = \Omega_2$ , and the two lasers are counter-propagating  $k_1 = -k_2$ , the expressions takes a simple form

$$H_0 = \nu a^\dagger a + \Delta (|g_B\rangle\langle g_B| + |g_D\rangle\langle g_D|) \quad (82)$$

$$H_I = \Omega \left( \cos(k\hat{x}) D_B^\dagger + \sin(k\hat{x}) D_D^\dagger \right) \quad (83)$$

$$\approx \Omega \left( D_B^\dagger + k\hat{x} D_D^\dagger \right). \quad (84)$$

In the LD regime, only the bright state is coupled to the excited state. To the zeroth order, the dark state is not coupled. But the dark state can be driven directly only after changing the motional state. This Hamiltonian now looks similar to the spin cooling case.

An interesting case is if, instead, the lasers are co-propagating with  $k_1 = k_2$ , then  $H_I = \Omega D_B^\dagger e^{ikx}$ , and the dark state is dark even to  $n$  changing transitions. Co-propagating light cannot change the momentum, prohibiting cooling.

Next, we can adiabatically eliminate the excited state using Eq. 15 and 16 to get the effective ground-state dynamics. In the original basis, the effective ground-state Hamiltonian is

$$\begin{aligned} H_{\text{eff}} &= \nu \hat{a}^\dagger \hat{a} (\Delta_1 - \frac{\Omega_1^2}{\Delta}) |g_1\rangle\langle g_1| + (\Delta_2 - \frac{\Omega_2^2}{\Delta}) |g_2\rangle\langle g_2| \\ &\quad - \frac{\Omega_1 \Omega_2}{\Delta} \left( |g_1\rangle\langle g_2| e^{i(k_2 - k_1)\hat{x}} + h.c. \right). \end{aligned} \quad (85)$$

In the bright and dark basis with  $\Omega_1 = \Omega_2$  and  $k_2 = -k_1$ , the effective ground-state Hamiltonian is

$$\begin{aligned} H_{\text{eff}} &= \nu a^\dagger a + \frac{\Omega_1^2 + \Omega_2^2}{2\Delta} |g_B\rangle\langle g_B| \\ &\quad + \left( ik\hat{x} \frac{\Omega_1 \Omega_2}{\Delta} |g_B\rangle\langle g_D| + h.c. \right) \end{aligned} \quad (86)$$

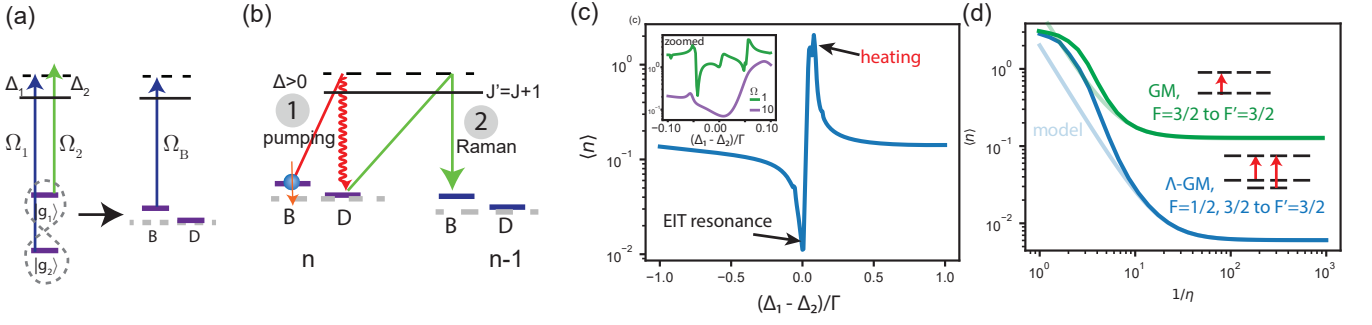


FIG. 7. (a) EIT and  $\Lambda$ -enhanced GM decrease temperature by establishing more dark states to cool into. (b) EIT cooling uses two lasers with Rabi frequencies  $\Omega_1$  and  $\Omega_2$  to drive a two-photon transition from  $|B, n\rangle$  to  $|D, n-1\rangle$ . (c) Simulations of population versus the two-photon detuning. Best cooling occurs at the two-photon resonance when  $\Delta_1 = \Delta_2$ . A heating resonance occurs to the right. Parameters are  $\eta = 0.05$ ,  $\Delta = 10\Gamma$ , and  $\Omega_1 = \Omega_2$ . The cooling power is set so that the light shift equals the trapping frequency. The inset shows that as the cooling power is lowered, the resonance shifts over. When the light shift becomes small compared to the trapping frequency, the two-photon detuning must compensate to drive  $n \rightarrow n-1$ . (d) Comparison of GM and  $\Lambda$ -GM. Light dashed is simple model from Eq. 73 with parameters  $\gamma_h/\gamma_+ = 2.0$  and  $\gamma_-/\gamma_+ = 0.006$  for  $\Lambda$ -GM, and  $\gamma_s/\gamma_+ = 5.0$  and  $\gamma_+/\gamma_- = 0.11$  for GM.

and the collapse operators are

$$L_{\text{eff}, \pm, i} = \frac{\sqrt{\Gamma} \Omega_{\text{rms}}}{\Delta - i\Gamma/2} \hat{D}_i \left( \hat{D}_B \pm ik\hat{x}(\hat{D}_B + \frac{2\Omega_1\Omega_2}{\Omega_{\text{rms}}^2} \hat{D}_D) \right). \quad (87)$$

We can now see that the Hamiltonian and collapse operator take a similar form as before. The position-independent Hamiltonian results in a light shift for only the bright state. Therefore, just like GM, EIT also works in the blue-detuned regime so that the dark state is lower energy. The position-dependent Hamiltonian results in coupling between neighboring motional states. The collapse operator also has a position-independent term, which optically pumps from the bright state to the dark state, and a position-dependent term from recoil heating. So if you are at two photon resonance condition ( $\Lambda$ -enhancement) in GM, the formalism and the effectiveness of  $\Lambda$ -GM is identical to EIT.

In Fig. 7(c), we plot the cooling performance as a function of detuning. In the main plot, the light shift is equal to the trapping frequency, so the optimal cooling occurs when  $\Delta_1 = \Delta_2$ . The inset shows the cooling performance as the cooling power is decreased. The relative detuning can be adjusted to bring the system back into resonance and recover the cooling efficiency. Fig. 7(d) compares the optimal cooling performance for the  $F = 1/2, 3/2$  to  $F' = 3/2$  system, with and without the  $\Lambda$ -enhancement (i.e., with and without the  $F = 1/2$  state). The inclusion of the  $F = 1/2$  state in the  $\Lambda$ -configuration significantly improves the cooling performance. The simulation results are also fitted to the theoretical model to extract the effective cooling parameters.

The effects of EIT on the cooling performance can now be clearly seen. By creating darker reservoir states, EIT decreases the effective asymmetry between the pumping rates,  $\gamma_-/\gamma_+$ . As a result, the fundamental limit for

EIT cooling is similar to that of GM cooling, but reduced by the factor by which the dark states are darker. The cooling efficiency still depends on the inverse square of the Lamb-Dicke parameter,  $1/\eta^2$ . In Fig. 7(d), we plot the cooling performance for the  $F = 1/2, 3/2$  to  $F' = 3/2$  system, comparing the cases with and without the  $F = 1/2$  state in the  $\Lambda$ -configuration leads to a significant improvement in the cooling efficiency, demonstrating the power of EIT in enhancing the performance of sub-Doppler cooling techniques.

#### D. Raman-sideband cooling

Raman sideband (RSB) cooling has achieved the highest ground-state populations in neutral atoms [22, 66, 67],

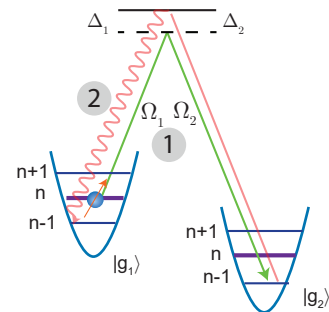


FIG. 8. Raman-sideband cooling. The first step is a Raman transition between spin states and decreasing the motional state by 1. The second step is spontaneous emission back to original spin, which keeps atom in  $n-1$  in the Lamb-Dicke regime. The cycle repeats until the population is in the ground-state.

ions [27], optical tweezers [24–26], and molecules [68, 69]. The working principle of RSB cooling is illustrated in Fig. 8(a).

In RSB cooling, two coherent, far-detuned lasers drive the transition from  $|g_1, n\rangle$  to  $|g_2, n-1\rangle$ , where  $|g_1\rangle$  and  $|g_2\rangle$  are two ground-states, and  $n$  represents the motional quantum number. The light shifts and scattering rates from these cooling lasers are typically negligible due to the large detuning. A third laser, tuned closer to resonance, performs optical pumping and exploits selection rules to ensure that the dark state remains dark.

The effective Raman coupling strength between the two ground-states is given by  $\Omega_1\Omega_2/\Delta$ , where  $\Omega_1$  and  $\Omega_2$  are the Rabi frequencies of the two cooling lasers, and  $\Delta$  is the detuning from the excited state. The effective ground-state Hamiltonian for RSB cooling is:

$$\langle g_1, n_1 | H_{\text{eff}} | g_2, n_2 \rangle = -\frac{\Omega_1\Omega_2}{\Delta} \langle n_1 | e^{i(k_1-k_2)\hat{x}} | n_2 \rangle, \quad (88)$$

where  $\hat{x}$  is the position operator, and  $k_1$  and  $k_2$  are the wave vectors of the two cooling lasers. By carefully tuning the laser frequencies and polarizations, this Raman coupling can be engineered to drive transitions that reduce the motional quantum number, leading to cooling.

In 3D, the Raman coupling term becomes  $e^{i(\mathbf{k}_1-\mathbf{k}_2)\cdot\hat{\mathbf{r}}} \approx 1 + i\hat{x}(\mathbf{k}_1-\mathbf{k}_2)\cdot\hat{\mathbf{x}}$ , which is related to the projection of the difference wave-vector onto the cooling axis. Multiple laser beams are typically used so that pairs of beams have projections on all three axes, enabling 3D cooling.

RSB cooling improves upon EIT and  $\Lambda$ -GM cooling techniques, which introduced dark states in an electromagnetically induced transparency (EIT) configuration. While EIT and  $\Lambda$ -GM achieved lower temperatures, they were limited by spontaneous emission from the dark state, parameterized by the ratio  $\eta^2\gamma_h/\gamma_+$ , where  $\eta$  is the Lamb-Dicke parameter,  $\gamma_h$  is the heating rate, and  $\gamma_+$  is the pumping rate.

RSB cooling addresses this limitation by increasing the detuning of the cooling lasers until the collapse operator  $L$  becomes negligible, effectively eliminating spontaneous emission and repumping from the cooling lasers. The additional repump beam, optimized using angular momentum selection rules, ensures that the state  $|g_1\rangle$  remains dark to it, making the dark state immune to position-dependent spontaneous emission.

An effective spin model for RSB cooling can be created, where the light shift from the cooling light is ignored, and the two-photon detuning is adjusted to bring the  $|g_1, n\rangle$  to  $|g_2, n-1\rangle$  transition into resonance:

$$H = \nu\hat{a}^\dagger\hat{a} + (\Delta_1 - \Delta_2)|g_2\rangle\langle g_2| + \Omega_R k \hat{x} \hat{F}_x \\ L_+ = \sqrt{\gamma_+} \hat{F}_+(1 + ik\hat{x}). \quad (89)$$

While RSB cooling offers significant advantages, its fundamental limitations are often technical rather than theoretical. The coherence time between the two ground-states is typically limited to a few milliseconds due to

factors such as magnetic field fluctuations or laser decoherence. For efficient cooling, the Raman Rabi frequency  $\Omega_R$  should exceed 10 kHz. However, the Rabi frequency for the  $n$  to  $n$  transition is larger than that of the  $n$  to  $n-1$  transition by a factor of  $1/\eta$ , resulting in both transitions being driven simultaneously. Further analysis is needed to determine the cooling limit in the presence of these technical constraints.

While RSB cooling offers a pathway to overcome the limitations of EIT and  $\Lambda$ -GM cooling schemes, its implementation is more complex experimentally. However, it potentially enables more efficient ground-state cooling in a wider range of atomic and molecular systems.

## V. ANALYSIS

The formalism in this paper reveals that all two-photon cooling schemes share a fundamental similarity: they involve a Raman transition between neighboring motional states with different spin states. Close-to-resonance cooling schemes like PG and GM utilize light shifts to bring the states into resonance, while further detuned cooling methods, such as Raman sideband (RSB) cooling, use the two-photon detuning of two frequencies and two far detuned ground-states. Similarly, techniques like  $\Lambda$ -GM cool by establishing dark states through destructive interference of two frequencies and two far detuned ground-states.

PG cooling is fundamentally limited to the optical pumping asymmetry, which for  $F$  to  $F+1$  is  $\langle n \rangle \approx 1$ . GM and  $\Lambda$ -GM lower the population to  $\langle n \rangle \approx \eta^2$ . But, spontaneous emission in these schemes still drives the population out of the dark state through either spontaneous emission from the first-order LD parameter or in the effective ground-state formalism, the position dependent component of the collapse operator. The dark  $n=0$  state is thus not completely dark, as it still can be driven through the  $n=1$  excited state. However, when using the Raman light in an optical pump, this is unpreventable, as the light requires a position-dependent term to produce the Raman coupling between motional states.

RSB cooling represents the ultimate limit of cooling, detuning so far from the excited state that the spontaneous emission of the Raman coupling light is negligible. The re-pumping is achieved through a separate spontaneous emission beam optimized to make the dark state truly dark.

In practical laboratory settings, PG, GM, and  $\Lambda$ -GM are more convenient due to their operational simplicity and similarity to the MOT configuration. But RSB is still employed for high ground-state preparation despite its significant experimental overhead. This paper demonstrates that Grey molasses cooling combined with the  $\Lambda$ -enhancement can achieve significant ground-state populations. This raises the question of how schemes resembling MOT configurations can be adapted for near-ground-state cooling. Likely, this adaptation involves



adding an additional beam specialized for optical pumping. For example adding an additional circularly polarized beam close-to-resonance beam for optical pumping (not counter-propagating). This should, from this model, provide the optical pumping without driving sidebands of the dark state. Then in the limit of large detuning for the GM beams, it would effectively create a  $L_+ = \sqrt{\gamma_+} e^{ik\hat{x}} \hat{F}_+$  from the RSB model. This will be the investigation of future experimental and theoretical work.

## VI. CONCLUSION

This study presents a comprehensive theoretical framework for major cooling mechanisms in neutral atom tweezers, uncovering shared principles across diverse techniques. Our approach combines detailed full-level structure simulations with a simplified spin model, offering novel insights for optimizing cooling schemes. By extending previous research to encompass arbitrary spins and polarizations, we show that gray molasses cooling may potentially reach the ground-state, challenging conventional limits and opening up new avenues for exploration.

Future research will investigate polarization gradients in three-dimensional beam configurations and examine deviations from the idealized one-dimensional cases presented here. We also plan to conduct simulations for specific alkali atoms, including all relevant ground and excited states, to assess the impact of multiple excited states and cross-coupling between lasers addressing different hyperfine ground-states. These simulations will help establish fundamental cooling limits for each atomic species for various techniques. Future research will explore innovative cooling approaches that blur the boundaries between established techniques.

Rapid, robust, and efficient ground-state optical cooling will increase the coherence and fidelity of experiments throughout the ultracold field. Reducing thermal motion in Rydberg atoms will pave the way for higher-fidelity quantum gates. Rapid optical cooling techniques could also reduce the long times associated with thermal evaporation for producing degenerate gases.

## ACKNOWLEDGEMENTS

This work was supported by the NSF Career Award (Award No. 0543784). We express our gratitude to Yichao Yu for valuable early discussions regarding the

relationship between spin cooling and Raman-sideband cooling.

## APPENDIX A

### Dipole spin operator

For the atom spin, we will use the hyperfine spin states  $\mathbf{F} = \mathbf{J} + \mathbf{I}$ . Note that setting  $I = 0$  recovers the  $J$  formalism for comparison. The excited states are  $|F_e, m_e\rangle$  and ground states are  $|F_g, m_g\rangle$ . The dipole operator in Eq. 5 is in this spin basis and using the Wigner-Eckart theorem is

$$\hat{D}_q = \sum_{m_g m_e} O_{IF_g F_e}^{J_g J_e} \langle F_g m_g | F_e m_e; 1q \rangle |F_g m_g\rangle \langle F_e m_e|. \quad (\text{A.90})$$

The oscillator strength coefficients are given by

$$O_{IF_g F_e}^{J_g J_e} = (-1)^{F_e + J_g + I + 1} \sqrt{(2F_e + 1)(2J_g + 1)} \left\{ \begin{matrix} J_e & J_g & 1 \\ F_g & F_e & I \end{matrix} \right\}, \quad (\text{A.91})$$

which are on the order of unity and give the strength of a  $F_g$  to  $F_e$  transition relative to the  $J_g$  to  $J_e$  transition with  $\sum_{F_e} |O_{IF_g F_e}^{J_g J_e}|^2 = 1$

### Spin tensor coefficients

The coefficients are determined by the Wigner-Eckart reduced matrix in the ground and excited spins. For the case of  $J, F$  in the ground and  $J', F'$  in the excited, the coefficients are [38]:

$$C^{(0)} = (-1)^{3F - F'} \sqrt{\frac{1}{3} \frac{2F' + 1}{\sqrt{2F + 1}}} \times \left( \begin{matrix} F & 1 & F' \\ 1 & F & 0 \end{matrix} \right) \left| \left\{ \begin{matrix} 1 & F & F' \\ 0 & 1/2 & F \end{matrix} \right\} \right|^2, \quad (\text{A.92})$$

$$C^{(1)} = (-1)^{3F - F'} \sqrt{\frac{3}{2} \frac{2F' + 1}{\sqrt{F(F + 1)(2F + 1)}}} \times \left( \begin{matrix} F & 1 & F' \\ 1 & F & 1 \end{matrix} \right) \left| \left\{ \begin{matrix} 1 & F & F' \\ 0 & 1/2 & F \end{matrix} \right\} \right|^2, \quad (\text{A.93})$$

$$C^{(2)} = (-1)^{3F - F'} \sqrt{\frac{30(2F' + 1)}{F(F + 1)(2F + 1)(2F - 1)(2F + 3)}} \times \left( \begin{matrix} F & 1 & F' \\ 2 & F & 0 \end{matrix} \right) \left| \left\{ \begin{matrix} 1 & F & F' \\ 0 & 1/2 & F \end{matrix} \right\} \right|^2. \quad (\text{A.94})$$

- 
- [1] A. M. Kaufman and K. K. Ni, Nat. Phys. **17**, 1324 (2021).  
 [2] D. Bluvstein, S. J. Evered, A. A. Geim, S. H. Li, H. Zhou, T. Manovitz, S. Ebadi, M. Cain, M. Kalinowski, D. Hangleiter, J. P. B. Ataiades, N. Maskara, I. Cong,

X. Gao, P. S. Rodriguez, T. Karolyshyn, G. Semeghini, M. J. Gullans, M. Greiner, V. Vuletić, and M. D. Lukin, Nature **626**, 58 (2024).

- [3] L. Anderegg, L. W. Cheuk, Y. Bao, S. Burchesky, W. Ketterle, K.-K. Ni, and J. M. Doyle, *Science* **365**, 1156 (2019).
- [4] Y. Bao, S. S. Yu, L. Anderegg, E. Chae, W. Ketterle, K.-K. Ni, and J. M. Doyle, *Science* **382**, 1138 (2023), <https://www.science.org/doi/pdf/10.1126/science.adf8999>.
- [5] D. K. Ruttley, A. Guttridge, T. R. Hepworth, and S. L. Cornish, *PRX Quantum* **5**, 020333 (2024).
- [6] J. T. Zhang, L. R. B. Picard, W. B. Cairncross, K. Wang, Y. Yu, F. Fang, and K.-K. Ni, *Quantum Sci. Technol.* **7**, 035006 (2022).
- [7] P. K. Molony, P. D. Gregory, Z. Ji, B. Lu, M. P. Köppinger, C. R. Le Sueur, C. L. Blackley, J. M. Hutson, and S. L. Cornish, *Phys. Rev. Lett.* **113**, 255301 (2014).
- [8] B. M. Spar, E. Guardado-Sanchez, S. Chi, Z. Z. Yan, and W. S. Bakr, *Phys. Rev. Lett.* **128**, 223202 (2022).
- [9] M. Holten, L. Bayha, K. Subramanian, C. Heintze, P. M. Preiss, and S. Jochim, *Phys. Rev. Lett.* **126**, 020401 (2021).
- [10] A. Cooper, J. P. Covey, I. S. Madjarov, S. G. Porsev, M. S. Safronova, and M. Endres, *Phys. Rev. X* **8**, 041055 (2018).
- [11] S. Saskin, J. T. Wilson, B. Grinkemeyer, and J. D. Thompson, *Phys. Rev. Lett.* **122**, 143002 (2019).
- [12] A. Jenkins, J. W. Lis, A. Senoo, W. F. McGrew, and A. M. Kaufman, *Phys. Rev. X* **12**, 021027 (2022).
- [13] J. Dalibard and C. Cohen-Tannoudji, *J. Opt. Soc. Am. B* **6**, 2023 (1989).
- [14] C. Tuchendler, A. M. Lance, A. Browaeys, Y. R. P. Sortais, and P. Grangier, *Phys. Rev. A* **78**, 033425 (2008).
- [15] B. J. Lester, N. Luick, A. M. Kaufman, C. M. Reynolds, and C. A. Regal, *Phys. Rev. Lett.* **115**, 073003 (2015).
- [16] M. Endres, H. Bernien, A. Keesling, H. Levine, E. R. Anschuetz, A. Krajenbrink, C. Senko, V. Vuletić, M. Greiner, and M. D. Lukin, *Science* **354**, 1024 (2016).
- [17] A. T. Grier, I. Ferrier-Barbut, B. S. Rem, M. Delehaye, L. Khaykovich, F. Chevy, and C. Salomon, *Phys. Rev. A* **87**, 063411 (2013).
- [18] A. T. Grier, I. Ferrier-Barbut, B. S. Rem, M. Delehaye, L. Khaykovich, F. Chevy, and C. Salomon, *Phys. Rev. A* **87**, 063411 (2013).
- [19] Y.-S. Chin, M. Steiner, and C. Kurtsiefer, *Phys. Rev. A* **96**, 033406 (2017).
- [20] M. O. Brown, T. Thiele, C. Kiehl, T.-W. Hsu, and C. A. Regal, *Phys. Rev. X* **9**, 011057 (2019).
- [21] K. N. Blodgett, D. Peana, S. S. Phatak, L. M. Terry, M. P. Montes, and J. D. Hood, *Phys. Rev. Lett.* **131**, 083001 (2023).
- [22] A. J. Kerman, V. Vuletić, C. Chin, and S. Chu, *Phys. Rev. Lett.* **84**, 439 (2000).
- [23] M. Popp, J.-J. Garcia-Ripoll, K. G. Vollbrecht, and J. I. Cirac, *Phys. Rev. A* **74**, 013622 (2006).
- [24] A. M. Kaufman, B. J. Lester, and C. A. Regal, *Phys. Rev. X* **2**, 041014 (2012).
- [25] J. D. Thompson, T. G. Tiecke, A. S. Zibrov, V. Vuletić, and M. D. Lukin, *Phys. Rev. Lett.* **110**, 133001 (2013).
- [26] Y. Yu, N. R. Hutzler, J. T. Zhang, L. R. Liu, J. D. Hood, T. Rosenband, and K.-K. Ni, *Phys. Rev. A* **97**, 063423 (2018).
- [27] C. Monroe, D. M. Meekhof, B. E. King, S. R. Jefferts, W. M. Itano, D. J. Wineland, and P. Gould, *Phys. Rev. Lett.* **75**, 4011 (1995).
- [28] A. Schliesser, R. Rivière, G. Anetsberger, O. Arcizet, and T. J. Kippenberg, *Nature Phys* **4**, 415 (2008).
- [29] E. Peik, J. Abel, T. Becker, J. von Zanthier, and H. Walther, *Phys. Rev. A* **60**, 439 (1999).
- [30] S. Stenholm, *Rev. Mod. Phys.* **58**, 699 (1986).
- [31] D. Leibfried, R. Blatt, C. Monroe, and D. Wineland, *Rev. Mod. Phys.* **75**, 281 (2003).
- [32] J. I. Cirac, R. Blatt, P. Zoller, and W. D. Phillips, *Phys. Rev. A* **46**, 2668 (1992).
- [33] D. J. Wineland, J. Dalibard, and C. Cohen-Tannoudji, *JOSA B* **9**, 32 (1992).
- [34] W. Phillips, *Laser Cooling, Optical Traps and Optical Molasses*, ed. by J. Dalibard, J.-M. Raimond, and J. Zinn-Justin (North Holland, Amsterdam, 1992).
- [35] K. Mølmer and Y. Castin, *Quantum Semiclass. Opt.* **8**, 49 (1996).
- [36] D. J. Wineland and W. M. Itano, *Phys. Rev. A* **20**, 1521 (1979).
- [37] J. Johansson, P. Nation, and F. Nori, *Comput. Phys. Commun.* **183**, 1760 (2012).
- [38] I. H. Deutsch and P. S. Jessen, *Optics Communications* **283**, 681 (2010), *quo vadis Quantum Optics?*
- [39] F. Reiter and A. S. Sørensen, *Phys. Rev. A* **85**, 032111 (2012).
- [40] J. Javanainen and S. Stenholm, *Appl. Phys.* **24**, 151 (1981).
- [41] H. Perrin, A. Kuhn, I. Bouchoule, and C. Salomon, *Europhys. Lett.* **42**, 395 (1998).
- [42] D.-J. Han, S. Wolf, S. Oliver, C. McCormick, M. T. DePue, and D. S. Weiss, *Phys. Rev. Lett.* **85**, 724 (2000).
- [43] J. I. Cirac, R. Blatt, A. S. Parkins, and P. Zoller, *Phys. Rev. A* **48**, 1434 (1993).
- [44] V. Vuletić, H. W. Chan, and A. T. Black, *Phys. Rev. A* **64**, 033405 (2001).
- [45] D. R. Leibbrandt, J. Labaziewicz, V. Vuletić, and I. L. Chuang, *Phys. Rev. Lett.* **103**, 103001 (2009).
- [46] M. A. Norcia, A. W. Young, and A. M. Kaufman, *Phys. Rev. X* **8**, 041054 (2018).
- [47] A. Cooper, J. P. Covey, I. S. Madjarov, S. G. Porsev, M. S. Safronova, and M. Endres, *Phys. Rev. X* **8**, 041055 (2018).
- [48] M. Saffman, *J. Phys. B: At. Mol. Opt. Phys.* **49**, 202001 (2016).
- [49] P. M. Duarte, R. A. Hart, J. M. Hitchcock, T. A. Corcovilos, T.-L. Yang, A. Reed, and R. G. Hulet, *Phys. Rev. A* **84**, 061406 (2011).
- [50] F. Berto, E. Perego, L. Duca, and C. Sias, *Phys. Rev. Res.* **3**, 043106 (2021).
- [51] R. Taieb, R. Dum, J. I. Cirac, P. Marte, and P. Zoller, *Phys. Rev. A* **49**, 4876 (1994).
- [52] M. Martinez-Dorantes, W. Alt, J. Gallego, S. Ghosh, L. Ratschbacher, and D. Meschede, *Phys. Rev. A* **97**, 023410 (2018).
- [53] A. A. Urech, *Single Strontium Atoms in Optical Tweezers*, Phd thesis, Van der Waals-Zeeman Institute, University of Amsterdam (2023).
- [54] J. P. Covey, I. S. Madjarov, A. Cooper, and M. Endres, *Phys. Rev. Lett.* **122**, 173201 (2019).
- [55] A. Urech, I. H. A. Knottnerus, R. J. C. Spreeuw, and F. Schreck, *Phys. Rev. Res.* **4**, 023245 (2022).
- [56] G. Morigi, J. Eschner, and C. H. Keitel, *Phys. Rev. Lett.* **85**, 4458 (2000).
- [57] P. D. Lett, R. N. Watts, C. I. Westbrook, W. D. Phillips, P. L. Gould, and H. J. Metcalf, *Phys. Rev. Lett.* **61**, 169 (1988).
- [58] Authors, *EPL* **100**, 63001 (2012).

- [59] D. Nath, R. K. Easwaran, G. Rajalakshmi, and C. S. Unnikrishnan, *Phys. Rev. A* **88**, 053407 (2013).
- [60] B. Darquié, M. P. A. Jones, J. Dingjan, J. Beugnon, S. Bergamini, Y. Sortais, G. Messin, A. Browaeys, and P. Grangier, *Science* **309**, 454 (2005), <https://www.science.org/doi/pdf/10.1126/science.1113394>.
- [61] J. Ang'ong'a, C. Huang, J. P. Covey, and B. Gadway, *Phys. Rev. Res.* **4**, 013240 (2022).
- [62] M. Joshi, A. Fabre, C. Maier, T. Brydges, D. Kiesenhofer, H. Hainzer, R. Blatt, and C. Roos, *New J. Phys.* **22**, 103013 (2020).
- [63] C. F. Roos, D. Leibfried, A. Mundt, F. Schmidt-Kaler, J. Eschner, and R. Blatt, *Phys. Rev. Lett.* **85**, 5547 (2000).
- [64] Y. Lin, J. P. Gaebler, T. R. Tan, R. Bowler, J. D. Jost, D. Leibfried, and D. J. Wineland, *Phys. Rev. Lett.* **110**, 153002 (2013).
- [65] L. W. Cheuk, L. Anderegg, B. L. Augenbraun, Y. Bao, S. Burchesky, W. Ketterle, and J. M. Doyle, *Phys. Rev. Lett.* **121**, 083201 (2018).
- [66] S. E. Hamann, D. L. Haycock, G. Klose, P. H. Pax, I. H. Deutsch, and P. S. Jessen, *Phys. Rev. Lett.* **80**, 4149 (1998).
- [67] A. J. Kerman, *Raman sideband cooling and cold atomic collisions in optical lattices*, Ph.d. thesis, Stanford University, Stanford, CA (2002), available online. Search ProQuest Dissertations & Theses.
- [68] Y. Bao, S. S. Yu, J. You, L. Anderegg, E. Chae, W. Ketterle, K.-K. Ni, and J. M. Doyle, arXiv preprint arXiv:2309.08706 (2023).
- [69] Y. Lu, S. J. Li, C. M. Holland, and L. W. Cheuk, *Nature Physics* **20**, 389 (2024).